



## THREE DIMENSIONAL FORMATION FLIGHT CONTROL

THESIS

James K. Hall  
Captain, USAF

AFIT/GAE/ENY/00M-06

*DEPARTMENT OF THE AIR FORCE*  
**AIR UNIVERSITY**

**AIR FORCE INSTITUTE OF TECHNOLOGY**

Wright-Patterson Air Force Base, Ohio

APPROVED FOR PUBLIC RELEASE; DISTRIBUTION UNLIMITED

**DTIC QUALITY INSPECTED 4**

20000803 141

AFIT/GAE/ENY/00M-06

**THREE DIMENSIONAL FORMATION FLIGHT CONTROL**

THESIS

James K. Hall  
Captain, USAF

AFIT/GAE/ENY/00M-06

Approved for public release; distribution unlimited

The views expressed in this thesis are those of the author and do not reflect the official policy or position of the United States Air Force, Department of Defense, or the U.S. Government.

THREE DIMENSIONAL FORMATION FLIGHT CONTROL

THESIS

Presented to the faculty of the Graduate School of Engineering and Management

of the Air Force Institute of Technology

Air University

In Partial Fulfillment of the

Requirements for the Degree of

Master of Science in Aeronautical Engineering

James K. Hall

Captain, USAF

March, 2000

Approved for Public Release; distribution unlimited

THREE DIMENSIONAL FORMATION FLIGHT CONTROL

James K. Hall, B.S.M.E.

Captain, USAF

Approved:

M. Pachter

Dr. Mier Pachter  
Thesis Committee Co-chairman

March 3, 2000

Date

Bradley S. Liebet

Dr. Bradley S. Liebet  
Thesis Committee Co-chairman

3 Mar 00

Date

Jeffery P. Bons

Jeffery P. Bons, Maj, USAF  
Committee Member

3 Mar 00

Date

## Acknowledgements

This document represents the culmination of many hours of intense study and numerous returns to basic textbooks to reinforce and solidify the knowledge and learning gained during my graduate level studies. This profound level of study and thought has given me a much more solid foundation in the basics of aerodynamics and controlling dynamic systems. I had been a bit unsure of the abilities I was taking to my next assignment, but the thesis process has given me priceless experience and understanding. I could not have arrived at this point without the guidance and help of numerous people, several of which I would like to acknowledge specifically.

I had reservations about asking an Electrical Engineering Professor to be on my thesis committee, but I now consider it divine Providence. Dr. Pachter has been a truly great teacher and mentor.

David Hopper was my constant ally against all challenges, whether it was understanding concepts, discussing problems, or just maintaining perspective. Greg Gilbreath unselfishly shared his amazing intellect and understanding. Ryan Pendleton was literally my MATLAB library throughout the thesis project. The keen mind and willing disposition of Bill Blake got me going on this project and provided assistance at critical junctures along the way.

My wife, my family, and my God gave me strength and courage to press forward each day. They are my life and my joy.

James K. Hall

# Table of Contents

	Page
Acknowledgements.....	i
Table of Contents.....	ii
List of Figures.....	iv
List of Tables .....	vi
List of Symbols.....	vii
Abstract.....	x
1 Introduction .....	1-1
2 Literature Review .....	2-1
2.1 History of Flying for Mutual Benefit.....	2-1
2.2 Close Formation Flight.....	2-2
2.2.1 Vortices Explained .....	2-2
2.2.2 Vortex Models.....	2-4
2.2.3 Formation Geometry.....	2-4
2.3 Automatic Formation Flight Control.....	2-6
3 Three Dimensional Formation Dynamics.....	3-1
3.1 Rotating Frame of Reference .....	3-1
3.2 Angular Rates .....	3-3
3.3 Kinematics.....	3-4
3.4 Formation Model Equations of Motion.....	3-8
3.5 Aerodynamic Interaction Effects .....	3-10
3.5.1 Vortex Effects on the Wing.....	3-10
3.5.2 Lift and Drag Analysis .....	3-16
3.5.3 Upwash Velocity Equations .....	3-19
3.5.4 Vortex Effects on the Vertical Tail.....	3-21
4 Formation Flight Controller.....	4-1
4.1 Controller Design .....	4-1
4.2 Formation Flight Turns .....	4-3
5 Formation Flight Simulation Results.....	5-1

5.1	Simulation Aircraft.....	5-1
5.2	Displacement Recovery Maneuvers.....	5-2
5.3	Velocity Change Maneuvers .....	5-7
5.4	Altitude Change Maneuvers.....	5-10
5.5	Heading Change Maneuvers .....	5-14
5.6	Climbing Turn Maneuver.....	5-26
5.7	Formation Flight Control System Gains .....	5-31
6	Conclusions and Recommendations.....	6-1
6.1	Conclusions .....	6-1
6.2	Recommendations .....	6-1
	Appendix A.....	1
	Bibliography .....	1
	Vita .....	1

## List of Figures

Figure 1. Velocity Distribution in Vortex of Viscous and Inviscid Flow .....	2-3
Figure 2. Two Aircraft Formation Schematic. ....	2-5
Figure 3. Inertial and Wing Axes. ....	3-2
Figure 4. Rotating Reference Frames (viewed from above). ....	3-5
Figure 5. Separation and Attitude in the L Reference Frame.....	3-12
Figure 6. Lift Vector Rotation on W Wing. ....	3-16
Figure 7. Vertical Tail of W in Vortex Interaction.....	3-22
Figure 8. Interaction Forces on the Vertical Tail (viewed from above).....	3-23
Figure 9. W displaced from the optimal position. ....	5-3
Figure 10. W displaced from optimal position: alternate control law .....	5-4
Figure 11. W displaced away from the optimal position. ....	5-5
Figure 12. W displaced from the new optimal position. ....	5-6
Figure 13. W's response to L velocity increase maneuver. ....	5-8
Figure 14. W's response to L velocity increase maneuver: alternate control law. ....	5-9
Figure 15. W's response to L velocity decrease maneuver.....	5-10
Figure 16. W's response to L altitude increase maneuver. ....	5-11
Figure 17. W's response to L altitude increase maneuver: alternate control law. ....	5-12
Figure 18. W's response to L altitude decrease maneuver. ....	5-13
Figure 19. L positive heading change maneuver.....	5-14
Figure 20. W's response to positive L heading change: x axis.....	5-15
Figure 21. W's response to positive L heading change: alternate control law: x axis....	5-16

Figure 22. W's response to positive L heading change: y axis.....	5-17
Figure 23. W's response to positive L heading change: alternate control law: y axis....	5-18
Figure 24. W's response to positive L heading change: z axis.....	5-19
Figure 25. W's response to positive L heading change: alternate control law: z axis. ....	5-20
Figure 26. W's response to positive L heading change: route formation: z axis. ....	5-21
Figure 27. L negative heading change maneuver.....	5-22
Figure 28. W's response to negative L heading change: x axis.....	5-23
Figure 29. W's response to negative L heading change: y axis.....	5-24
Figure 30. W's response to negative L heading change: z axis. ....	5-25
Figure 31. Flight path in climbing turn maneuver: inertial reference frame. ....	5-26
Figure 32. L simultaneous altitude and heading change maneuver.....	5-27
Figure 33. W's response to the climbing turn maneuver: x axis. ....	5-28
Figure 34. W's response to the climbing turn maneuver: y axis.....	5-29
Figure 35. W's response to the climbing turn maneuver: z axis.....	5-30

## List of Tables

Table 1	F-16 Class Aircraft Specifications .....	5-1
Table 2	Formation Flight Control System Gains .....	5-31

## List of Symbols

Symbol	Description
AR	Aspect Ratio
$b$	Wing Span
$b_v$	Span Between Trailing Vortices
$C$	Linear Transformation Matrix; Coefficient
$D$	Drag
$D_t$	Substantial Derivative
$g$	Acceleration of Gravity
$h$	Altitude
$K$	Gain Constant; Drag Polar Constant
$L$	Lift, First Aircraft in Formation (Leader)
$\ell$	Single Axis of Rotation Matrix
$M$	Mach Number
$m$	Mass
$P$	Roll Rate
$p$	Time Derivative of Roll Angle
$Q$	Pitch Rate
$q$	Dynamic Pressure
$R$	Position Vector; Yaw Rate
$r$	Distance
$S$	Surface Area
$T$	Thrust
$u$	$x$ Component of Velocity
$V$	Velocity

## List of Symbols

Symbol	Description
$v$	y Component of Velocity
$W$	Second Aircraft in Formation (Wingman)
$w$	z Component of Velocity
$x$	Aircraft Separation in the x-direction
$Y$	Side Force
$y$	Aircraft Separation in the y-direction
$z$	Aircraft Separation in the z-direction
$\Delta$	Change
$\Gamma$	Circulation
$\alpha$	Angle of Attack
$\beta$	Side Slip Angle
$\gamma$	Flight Path Angle
$\varepsilon$	Vortex Influenced Angle of Attack
$\eta$	Position of Vortex Filaments, Efficiency Factor
$\phi$	Roll Angle
$\theta$	Angle
$\sigma$	Distance Function
$\tau$	Time Constant
$\xi$	Integration Variable for Length
$\rho$	Density
$\omega$	Angular Velocity
$\psi$	Heading Angle

# List of Symbols

Symbol	Description
<b>Subscripts</b>	
a	Aerodynamic Coupling
c	Viscous Effects of Vortex Core, Commanded Geometry
D	Derivative
DD	Second Derivative
Do	Drag Polar
e	Error
I	Inertial Reference Frame, Integral
L	Rotating Reference Frame of the Leader
o	Original Configuration
P	Proportional
v	Vortex
vort	Vortex
vt	Vertical Tail
W	Rotating Reference Frame of the Wingman
$\alpha$	Lift Curve Slope
$\infty$	Freestream
1, 2	Vortex Filament Index

## **Abstract**

Automating the control of an aircraft flying in formation necessitates the extension of the theory of formation flight control to allow for three dimensional maneuvers. The formation was modeled as a two-aircraft, leader and wingman, formation. Both aircraft has its own three dimensional, rotating and translating, Cartesian axes system, with special attention being given to the motion of the leader in relation to the wingman. The controller operated using the equations of motion expressed in the rotating reference frame of the wing aircraft. The control system has seven states, three inputs and three disturbance signals to model the dynamics of the formation in three dimensional space. The control law employed was the feedback of the difference between in actual separation distance and the commanded separation distance to affect changes in thrust, lift, and roll rate. The control system incorporated proportional, integral, and derivative control elements, each with separate gains, to achieve and maintain the specified formation geometry despite various maneuvers flown by the leader. Simulated maneuvers included: an initial displacement of the wingman away from the formation geometry, and changes in the leader's velocity, altitude, and heading. For each maneuver, the controller performance was sufficient to maintain the commanded formation geometry.

# **THREE DIMENSIONAL FORMATION FLIGHT CONTROL**

## **1 Introduction**

Migrating geese have for centuries flown in formation to take advantage of the air flowing off of the wings of preceding birds to reduce induced drag. During World War I, when military aviation was first taking to the air, the United States Navy employed the idea of multiple aircraft flying together for mutual benefit when it hung pursuit planes from the dirigibles AKRON and MACON. The lessons learned during the air campaign over Germany during World War II, concerning the importance of fighter escort for strategic bombers, brought about research programs such as FICON and wingtip coupling that attempted to physically attach fighters to bombers. Today, as the USAF turns to an Air Expeditionary Force mode of operations, the opportunity for mutually beneficial flight is ripe by applying the concept of flying aircraft in close formation. Pilots have the ability to fly in very precise formations, however, asking a pilot to accomplish this task continuously for several hours is unrealistic. Hence, this research seeks to further the development of an automatic close formation flight control system for the wing aircraft by extending previous work to include full three dimensional aircraft formation dynamics. An automatic formation controller which entails proportional, integral, and derivative control action is designed, and its performance is examined by way of multiple simulated maneuvers.

## **2 Literature Review**

The background references reviewed for this research fit into three categories. The first category was an exploration of the history of flying for mutual benefit. The second pertained to aerodynamic interaction considerations for formation flight. The final category related to previous formation control system investigations.

### **2.1 History of Flying for Mutual Benefit**

In reference [1], several concepts for flying together were expounded. The first such concept appears to have been evaluated by the Navy, who created special attach points on the dirigibles AKRON and MACON, from which pursuit aircraft were hung. This combination of aircraft could loiter over hostile territory for reconnaissance purposes and also protect itself from enemy aircraft. Providing fighter escort for a bomber flying long duration missions was the impetus for the FICON (fighter conveyor) project described in [1]. The conveyor aircraft was the massive B-36 outfitted with an elaborate trapeze mechanism to which the fighter was attached and then hoisted into the bomb bay. The fighter was the XF-85, an egg-shaped, jet-propelled, folding-wing, landing-gearless experimental aircraft that proved too unstable to consistently reattach itself to the conveyor after flying its mission. The TOM-TOM project followed up on the FICON idea, but this time the fighter, an F-84, had its wings remain outside of the B-36 fuselage.

The wingtip coupling experiments described in [2] are interesting not only from the perspective of mutually beneficial flight, but also from a control system point of view. The principle underlying the wingtip coupling concept was to extend the range of several aircraft by connecting them together at the wingtips, thereby effectively creating a single aircraft with a very large aspect ratio. Early work with a C-47A and a Q-14B was very successful, and the program was extended to a B-29 and two F-84 aircraft. Numerous flights were accomplished, but always with the fighter pilots constantly controlling the flight of their aircraft. The next step in the program was an attempt to allow the F-84 aircraft's automatic flight control system to maintain proper flight attitude. Tragically, the control system was unable to properly adjust for the aerodynamic effects of flying coupled to the B-29, and both aircraft were destroyed and the aircrews killed.

## **2.2 Close Formation Flight**

The mutually beneficial flight concept explored in this research is called close formation flight. The benefit comes in the form of reducing the induced drag, achieved by flying aircraft in a specific formation so as to capitalize on the aerodynamic interaction with the vortices emanating from the leading aircraft's wings.

### **2.2.1 *Vortices Explained***

Vortices for aircraft in steady, level flight can be visualized as a pair of horizontal rotational air flows that start near the wingtips. Vortices are defined by two properties, vorticity and circulation. Kuethe and Chow [3] developed mathematical expressions for these properties in an ideal, inviscid flow. Vorticity is defined as the rotation of a fluid

flow about a point and is measured in units of length per time, whereas circulation is defined as the strength of the rotation and has units of length squared divided by time. Crow [4] proposed a stability theory for trailing vortices, however, for close formation flight, vortex instability is not an issue because of the relatively tight aircraft spacing. In Kopp [5], the formula for velocity distribution in a viscous fluid is presented. Rather than having infinite vorticity at the axis of rotation as seen in the inviscid model, the expression shows zero velocity at the vortex center. Figure 1 shows sample velocity distributions for the two different models. Note that as the radius increases, the two models yield similar answers. The velocity distribution in Figure 1 is found by treating the vortex as a filament at the center of rotation.

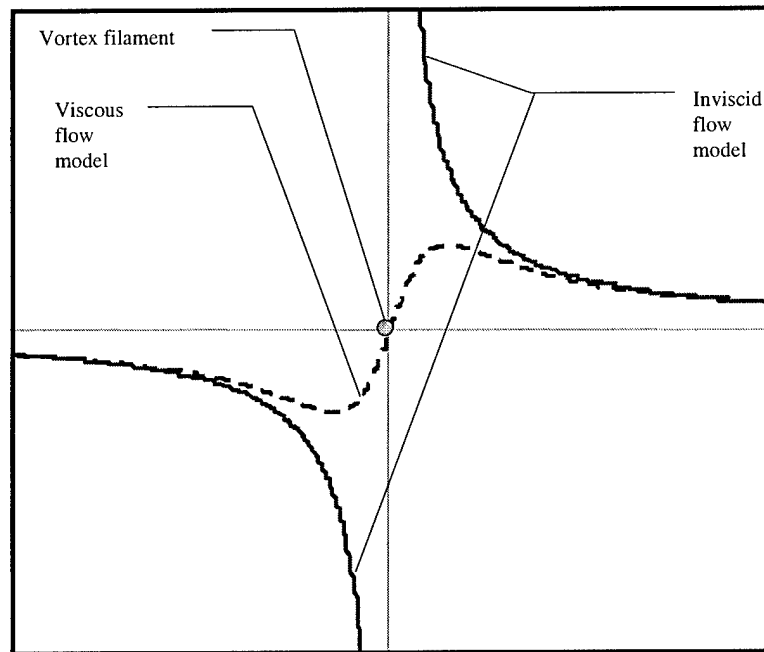


**Figure 1. Velocity Distribution in Vortex of Viscous and Inviscid Flow**

### **2.2.2 Vortex Models**

It is known that an aircraft creates a wake of vortex flow from each wing, however some difficulty arises in modeling the flow. One such model is called a horse shoe vortex, where the wing is replaced with a bound vortex and vortex filaments extend rearward and are connected at an infinite distance by another filament to complete a circuit in keeping with the Helmholtz laws. Other options are to model the aircraft wake as flat sheets of individual vortices or as a rolled up sheet of vortices as demonstrated by Beukenberg and Hummel [6]. Rather than an analytical model, Maskew [7] developed a numerical method called vortex lattice calculations to compute the flow properties of an airplane wake. In this research, the wake was modeled as a simple horse shoe vortex as in Proud [8] and Blake [10], allowing for the derivation of a relatively simple analytical expression for the vortex flow.

### **2.2.3 Formation Geometry**

The key to reaping the benefits of close formation flight is to fly in the correct position with respect to the vortex flow. There have been several studies conducted to determine the optimum aircraft location relative to one another in the formation. The optimum position for the purposes of this report is defined as producing maximum induced drag reduction while at the same time keeping a safety margin of longitudinal and lateral spacing to prevent collisions. Figure 2 provides an explanation of spacing terminology essential to understanding the discussion of formation geometry. For longitudinal spacing in an echelon formation, Maskew [7] proposed three span lengths was best because that is where the upwash reached a maximum value. Beukenberg [6]

and Myatt [11] both place the lateral spacing in such a way that wing tips actually overlap slightly to produce maximum upwash on the trailing aircraft. The work presented in [10] shows that maximum drag reduction is achieved when the formation is all in the same vertical plane during steady level flight. Therefore, in this research the formation geometry has a vertical spacing ( $z_c$ ) of zero (referring to Figure 2,  $z_L=0$ ), a longitudinal separation distance ( $x_c$ ) of three times the wing span of the leader and a lateral separation distance ( $y_c$ ) of  $\pi/4$  times the wing span of the leader. It can be seen that the separation in the x direction provides a safety margin to counteract the wing tip overlap in the y direction.

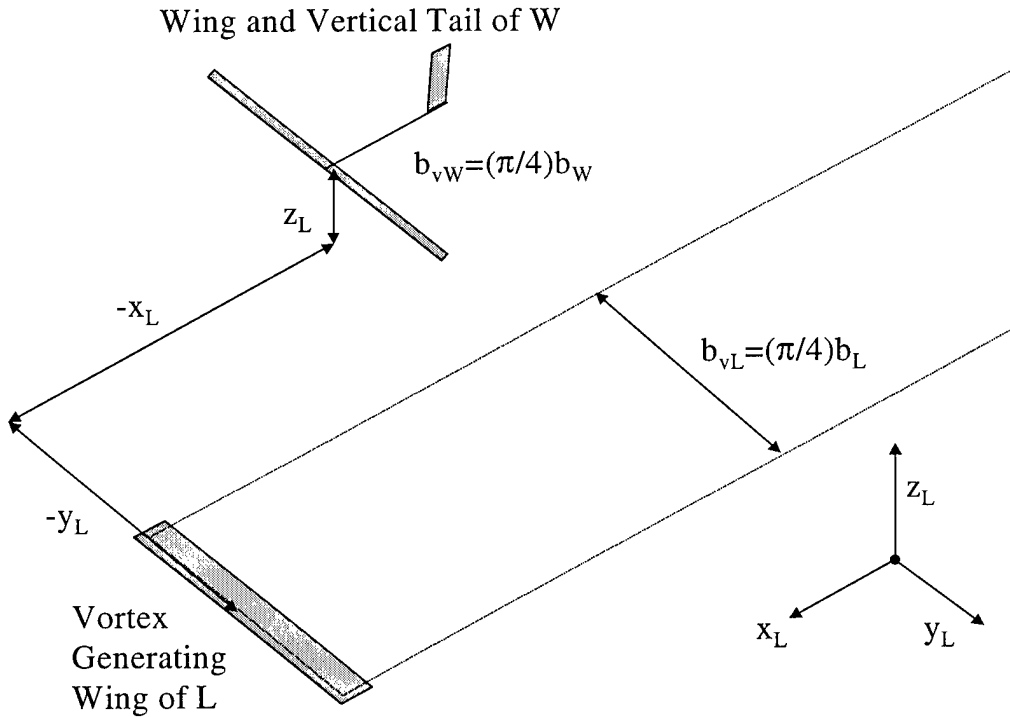


**Figure 2. Two Aircraft Formation Schematic.**

## **2.3 Automatic Formation Flight Control**

The work presented in [8], [9], and [12] modeled two aircraft that were fixed into a single orientation, thereby making the controller design problem essentially two dimensional. The linearization of the equations of motion allowed a proportional-integral (PI) control system to be designed using state space techniques. The control law developed in [8] was used as the starting point for the design of the three dimensional formation flight control system.

### 3 Three Dimensional Formation Dynamics

#### 3.1 Rotating Frame of Reference

Formation flight control necessitates the use of rotating frames of reference. Subscript W refers to the number two or wingman aircraft in the formation and subscript L refers to the aircraft leading the formation.

Each aircraft is considered as a point mass for developing the dynamic model. Each aircraft is treated as a single horseshoe vortex, with the trailing vortices separated by  $\pi/4$  times the span of the wing and emanating from the tips of the bound vortex that simulates the wing. Myatt, reference [11], shows that the lift distribution is approximately elliptical, which validates the use of  $\pi/4$  times the span of the wing as the distance between the vortex filaments.

The equations of motion are derived using a translating and rotating frame of reference at the instantaneous position of W. The rotating frame of reference is a triad of wind axes defined as follows: the x-axis aligned with the aircraft velocity vector, the z-axis aligned with the lift vector, and the y-axis (approximately out the left wing) completes the right-handed coordinate system. The derivation assumes no aerodynamic side force in the absence of the L vortex filaments, which means no sideslip is allowed, or in other words, coordinated flight.

The kinematics are based on the rotation from an inertial reference frame to a wind axes system attached to the W or L aircraft, subscripted according to which aircraft is being considered.

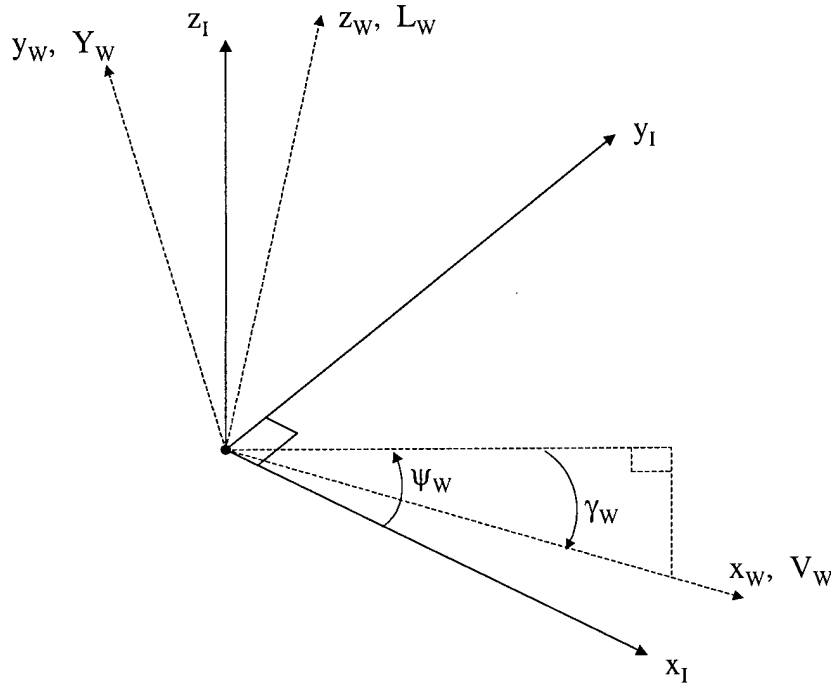


**Figure 3. Inertial and Wing Axes.**

The wind axes frame is specified by the  $\psi$ ,  $\gamma$ , and  $\phi$  Euler angles. For the sake of clarity, the final rotation, about the  $x_W$  axis and through the angle  $\phi$ , is not explicitly shown in Figure 3.

The orientation of the velocity vector,  $V_W$ , of the wing aircraft is specified by heading angle,  $\psi_W$ , and flight path angle,  $\gamma_W$ . The lift vector,  $L_W$ , is rotated by flight path angle,  $\gamma_W$ , and roll angle,  $\phi_W$ . An aerodynamic side force resulting from the vortex

filaments of  $L$ ,  $Y_w$ , is in the direction of  $y_w$ , and is included in the derivation to allow for the aerodynamic interaction of close formation flight. Since a point mass model is used, moments are not included in the analysis.

The three control variables are lift, thrust, and roll rate, and are denoted  $L_w$ ,  $T_w$ , and  $p_w$ , respectively. The state variables are  $V_w$  and the Euler angles  $\psi_w$  and  $\gamma_w$ .

### 3.2 Angular Rates

Expressions for the rate of change of the three state variables can be derived from Newton's Laws. Note that the positive sign in front of the weight term in equation (3.2.1) and the negative sign in front of the lift term of equation (3.2.2) result from our definition of positive flight path angle, as shown in Figure 3. Also, note that lift and side force are adjusted by bank angle,  $\phi_w$ .

$$\dot{V}_w = \frac{T_w - D_w}{m_w} + g \sin \gamma_w \quad (3.2.1)$$

$$\dot{\gamma}_w = -\frac{L_w \cos \phi_w}{m_w V_w} + \frac{g \cos \gamma_w}{V_w} - \frac{Y_w \sin \phi_w}{m_w V_w} \quad (3.2.2)$$

$$\dot{\psi}_w = -\frac{L_w \sin \phi_w}{m_w V_w \cos \gamma_w} + \frac{Y_w \cos \phi_w}{m_w V_w \cos \gamma_w} \quad (3.2.3)$$

Resolved into the frame of reference of the wing aircraft, the instantaneous angular rate,  $\vec{\omega}_w$ , of the W-wind axes triad is,

$$\vec{\omega}_w = \begin{bmatrix} P_w \\ Q_w \\ R_w \end{bmatrix} \quad (3.2.4)$$

From [13], with flight path angle substituted for pitch angle, the above angular rates are related to the Euler angle time derivatives according to the following transformation,

$$\begin{bmatrix} P \\ Q \\ R \end{bmatrix} = \begin{bmatrix} 1 & 0 & -\sin \gamma \\ 0 & \cos \phi & \sin \phi \cos \gamma \\ 0 & -\sin \phi & \cos \phi \cos \gamma \end{bmatrix} \begin{bmatrix} \dot{\phi} \\ \dot{\gamma} \\ \dot{\psi} \end{bmatrix} \quad (3.2.5)$$

Substituting the relationships for the change in flight path and heading angles into equation (3.2.5) and completing the matrix multiplication yields the following equations for the angular rates of the W-axes system:

$$P_w = \dot{\phi}_w + \frac{\tan \gamma_w (L_w \sin \phi_w - Y_w \cos \phi_w)}{m_w V_w} \quad (3.2.6)$$

$$Q_w = -\frac{L_w}{m_w V_w} + \frac{g \cos \gamma_w \cos \phi_w}{V_w} \quad (3.2.7)$$

$$R_w = -\frac{g \cos \gamma_w \sin \phi_w}{V_w} + \frac{Y_w}{m_w V_w} \quad (3.2.8)$$

### 3.3 Kinematics

Fundamental to the problem of formation flight is the relative position of L with respect to W. The position and attitude of both aircraft's wind axes need to be related to an inertial reference frame, subscripted I. Figure 4 shows the vector relationship, shown in two dimensions for clarity, between the inertial and the rotating axes systems.

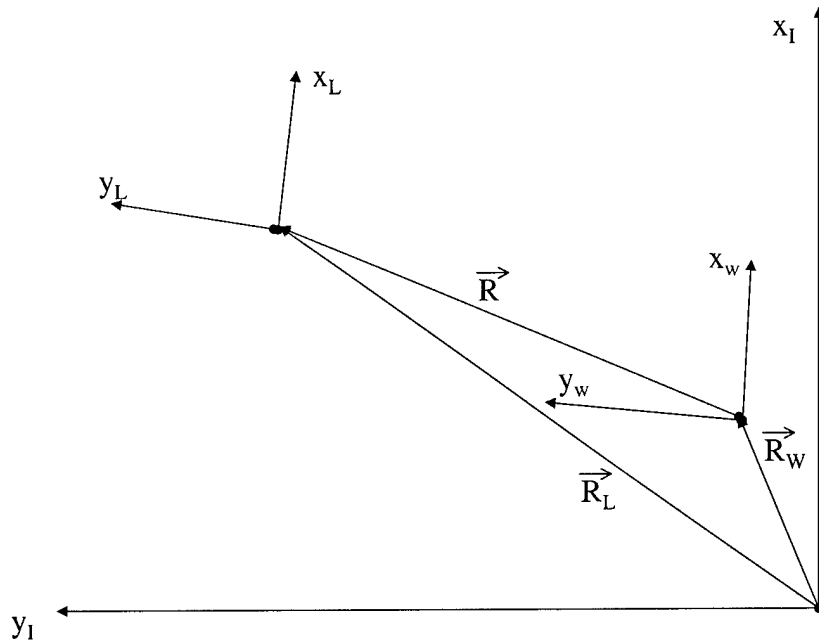


**Figure 4. Rotating Reference Frames (viewed from above).**

From Figure 4, the following vector expressions are developed, where the vectors  $\vec{R}_L$  and  $\vec{R}_W$  are resolved into the inertial reference frame and the vector  $\vec{R}$  is resolved in the rotating frame attached to W:

$$\vec{R}_L = \vec{R}_W + \vec{R}$$

Therefore the rate of change of the vectors can also be written;

$$\frac{D\vec{R}_L}{Dt} = \frac{D\vec{R}_W}{Dt} + \frac{D\vec{R}}{Dt}$$

where the change in relative position ( $\vec{R}$ ) in W's rotating reference frame can be transferred to the inertial reference frame using the following relationship,

$$\frac{D\vec{R}}{Dt} = \frac{d\vec{R}}{dt} + \vec{\omega}_w \times \vec{R} \quad (3.3.1)$$

The frame's angular velocity,  $\vec{\omega}_w$ , is defined in equation (3.2.4). Therefore equation (3.3.1) can be rewritten as follows:

$$\frac{D\vec{R}_L}{Dt} = \frac{D\vec{R}_w}{Dt} + \frac{d\vec{R}}{dt} + \vec{\omega}_w \times \vec{R} \quad (3.3.2)$$

Also, the rate of change in separation  $\vec{R}$ , can be written as the time derivative of the Cartesian components of the separation distance,

$$\frac{d\vec{R}}{dt} = \begin{bmatrix} \dot{x}_w \\ \dot{y}_w \\ \dot{z}_w \end{bmatrix} \quad (3.3.3)$$

The orientation of the rotating reference frame with respect to the inertial frame is specified by the  $\psi$ ,  $\gamma$ , and  $\phi$  Euler angles. The three individual single-axis-of-rotation transformation matrices are in the 3-2-1 rotation order or, in other words, first yaw, then pitch, followed by roll.

$$\ell_\psi = \begin{bmatrix} \cos\psi & -\sin\psi & 0 \\ \sin\psi & \cos\psi & 0 \\ 0 & 0 & 1 \end{bmatrix} \quad \ell_\gamma = \begin{bmatrix} \cos\gamma & 0 & \sin\gamma \\ 0 & 1 & 0 \\ -\sin\gamma & 0 & \cos\gamma \end{bmatrix} \quad \ell_\phi = \begin{bmatrix} 1 & 0 & 0 \\ 0 & \cos\phi & -\sin\phi \\ 0 & \sin\phi & \cos\phi \end{bmatrix}$$

The generic transformation matrix,  $C$ , is formed by multiplying the three single-axis-of-rotation matrices, viz.,

$$C = \begin{bmatrix} \cos\psi \cos\gamma & \cos\psi \sin\gamma \sin\phi - \sin\psi \cos\phi & \sin\psi \sin\phi + \cos\psi \sin\gamma \cos\phi \\ \sin\psi \cos\gamma & \cos\psi \cos\phi + \sin\psi \sin\gamma \sin\phi & -\cos\psi \sin\phi + \sin\psi \sin\gamma \cos\phi \\ -\sin\gamma & \cos\gamma \sin\phi & \cos\gamma \cos\phi \end{bmatrix}$$

The preceding transformation matrix is applicable to both L and W, with the only difference being the Euler angles used. The transformation from the L rotating reference

frame to inertial is denoted as  $C_L^I$ , and from the W rotating reference frame to inertial as  $C_W^I$ . Using the transformation matrix,  $C_W^I$ , the velocity relationship from equation (3.3.2) can be written in the inertial reference frame as,

$$V_L \begin{bmatrix} \cos \gamma_L \cos \psi_L \\ \cos \gamma_L \sin \psi_L \\ -\sin \gamma_L \end{bmatrix} = V_W \begin{bmatrix} \cos \gamma_W \cos \psi_W \\ \cos \gamma_W \sin \psi_W \\ -\sin \gamma_W \end{bmatrix} + C_W^I \left( \frac{d\vec{R}}{dt} + \vec{\omega}_W \times \vec{R} \right)$$

Solving the preceding equation for the rate of change in separation distance gives,

$$\frac{d\vec{R}}{dt} = -(\vec{\omega}_W \times \vec{R}) + C_W^{I^T} \left( V_L \begin{bmatrix} \cos \gamma_L \cos \psi_L \\ \cos \gamma_L \sin \psi_L \\ -\sin \gamma_L \end{bmatrix} - V_W \begin{bmatrix} \cos \gamma_W \cos \psi_W \\ \cos \gamma_W \sin \psi_W \\ -\sin \gamma_W \end{bmatrix} \right) \quad (3.3.4)$$

Using equations (3.2.4) and (3.3.2), the matrix operations can be performed to yield,

$$\begin{bmatrix} \dot{x} \\ \dot{y} \\ \dot{z} \end{bmatrix} = \begin{bmatrix} R_W y - Q_W z \\ P_W z - R_W x \\ Q_W x - P_W y \end{bmatrix} + V_L C_W^{I^T} \begin{bmatrix} \cos \gamma_L \cos \psi_L \\ \cos \gamma_L \sin \psi_L \\ -\sin \gamma_L \end{bmatrix} - V_W \begin{bmatrix} 1 \\ 0 \\ 0 \end{bmatrix} \quad (3.3.5)$$

where the vector that transforms the velocity of L into the W reference frame is,

$$\begin{bmatrix} \cos \gamma_W \cos \gamma_L \cos \psi_e + \sin \gamma_W \sin \gamma_L \\ \cos \gamma_L \sin \gamma_W \sin \phi_W \cos \psi_e + \cos \gamma_L \cos \phi_W \sin \psi_e - \cos \gamma_W \sin \gamma_L \sin \phi_W \\ \cos \gamma_L \sin \gamma_W \sin \phi_W \cos \psi_e - \cos \gamma_L \cos \phi_W \sin \psi_e - \cos \gamma_W \sin \gamma_L \sin \phi_W \end{bmatrix}$$

In the transformation vector above, the angle  $\psi_e$  is the heading error, defined as the difference between the L and W heading angles as shown below.

$$\psi_e = \psi_L - \psi_W$$

### 3.4 Formation Model Equations of Motion

The pertinent equations of motion for a two-aircraft formation model relate the velocities and attitudes of the wingman and the leader and the distance separating them. Thus, the state variables in the formation flight control system are:  $V_w$ ,  $\gamma_w$ ,  $\psi_w$ ,  $\phi_w$ ,  $x$ ,  $y$ ,  $z$ ,  $V_L$ ,  $\gamma_L$ , and  $\psi_L$  ( $\in \mathfrak{R}^{10}$ ), and the number of differential equations is ten. The three control variables for the controller are:  $L_w$ ,  $T_w$ , and  $p_w$  ( $\in \mathfrak{R}^3$ ), where  $p_w$  is defined as the time rate of change of W's bank angle,  $\dot{\phi}_w$ . However, the creation of a heading error state as shown above reduces the dimension of the system by one. An additional simplification can be made to the control system by declaring L's states exogeneous disturbances. Hence, the three model disturbances would be L's velocity, heading angle, and the y component of lift:  $V_L$ ,  $\gamma_L$ , and  $L_L \sin \phi_L$ . In this way, the original system model of ten states is reduced to the following seven states:  $V_w$ ,  $\gamma_w$ ,  $\phi_w$ ,  $\psi_e$ ,  $x$ ,  $y$ , and  $z$  ( $\in \mathfrak{R}^7$ ). The seven differential equations of motion that model the two-aircraft system are as follows:

$$\dot{V}_w = \frac{T_w - D_w}{m_w} + g \sin \gamma_w \quad (3.4.1)$$

$$\dot{\gamma}_w = -\frac{L_w \cos \phi_w - Y_w \sin \phi_w}{m_w V_w} + \frac{g \cos \gamma_w}{V_w} \quad (3.4.2)$$

$$\dot{\phi}_w = p_w \quad (3.4.3)$$

$$\dot{\psi}_e = -\frac{L_L \sin \phi_L}{m_L V_L \cos \gamma_L} + \frac{L_w \sin \phi_w - Y_w \cos \phi_w}{m_w V_w \cos \gamma_w} \quad (3.4.4)$$

$$\dot{x}_w = \frac{-yg \cos \gamma_w \sin \phi_w - zg \cos \gamma_w \cos \phi_w}{V_w} + \frac{zL_w + yY_w}{m_w V_w} - V_w \quad (3.4.5)$$

$$+ V_L (\cos \gamma_w \cos \gamma_L \cos \psi_e + \sin \gamma_w \sin \gamma_L)$$

$$\dot{y}_w = zp_w - \frac{z \tan \gamma_w (L_w \sin \phi_w - Y_w \cos \phi_w) - xY_w}{m_w V_w} + \frac{xg \cos \gamma_w \cos \phi_w}{V_w} \quad (3.4.6)$$

$$+ V_L (\sin \gamma_w \cos \gamma_L \sin \phi_w \cos \psi_e + \cos \gamma_L \sin \phi_w \sin \psi_e - \cos \gamma_w \sin \gamma_L \cos \phi_w)$$

$$\dot{z}_w = -yp_w - \frac{y \tan \gamma_w (L_w \sin \phi_w - Y_w \cos \phi_w) - xL_w}{m_w V_w} + \frac{xg \cos \gamma_w \cos \phi_w}{V_w} \quad (3.4.7)$$

$$+ V_L (\sin \gamma_w \cos \gamma_L \cos \phi_w \cos \psi_e - \cos \gamma_L \sin \phi_w \sin \psi_e - \cos \gamma_w \sin \gamma_L \cos \phi_w)$$

The drag,  $D_w$ , can be eliminated from the velocity equation (3.4.1) according to the following derivation. Using the definition of the coefficients of lift and drag, an expression for the drag force, as a function of lift, can be found.

$$\frac{D}{C_D} = qS = \frac{L}{C_L}$$

where,

$$q \equiv \frac{1}{2} \rho V^2$$

As in the example on page 217 of reference [14], the total drag coefficient can be found using the following equation:

$$C_D = C_{D_o} + KC_L^2$$

Substituting into the expression for drag gives,

$$D = \left( \frac{C_{D_o} + K \left( \frac{L}{qS} \right)^2}{\frac{L}{qS}} \right) L$$

which when applied to W yields,

$$D_W = \left( C_{D_{\alpha_W}} + K_W \left( \frac{L_W}{q_W S_W} \right)^2 \right) q_W S_W$$

Substituting this expression into equation (3.4.1) yields a new velocity relationship.

$$\dot{V}_W = \frac{1}{m_W} \left( T_W - q_W S_W C_{D_{\alpha_W}} - \frac{K_W L_W^2}{q_W S_W} \right) + g \sin \gamma_W \quad (3.4.8)$$

Equations (3.4.2) – (3.4.4) and equation (3.4.8) entail the point mass modeling of W using wind axes coordinate system definitions, and equations (3.4.5) – (3.4.7) are the change in separation distances measured in the W reference frame obtained from equation (3.3.5).

### 3.5 Aerodynamic Interaction Effects

#### 3.5.1 Vortex Effects on the Wing

The effect of vortices on the wing of W is a function of the separation distance between the two aircraft and their respective attitudes. Figure 2 shows the two-ship aircraft formation with the vortices trailing from L, and the aerodynamic surfaces of W's wing and vertical tail, all in L's rotating reference frame. The separation distance vector,  $\vec{R}$ , between aircraft can be transformed from the W rotating reference frame into the L frame using the following matrix multiplication:

$$\vec{R}_{WL} = -C_I^L C_W^I \vec{R}$$

where,

$$C_I^L = C_L^{I^T}$$

Again treating the wing of W as a lifting line, as in [9], and assuming no yawing of W, the attitude of W is specified by the y-axis of the W rotating reference frame and can be resolved into the L frame of reference. Points along the wing line of W can be written as,

$$\xi_L = -C_I^L C_W^I \begin{bmatrix} 0 \\ 1 \\ 0 \end{bmatrix} \xi$$

Because W's wing is being treated as a lifting line, the limits of  $\xi$  are the span between the locations of the trailing legs of the horseshoe vortex,  $b_{vW}$ . In the L frame of reference, the location of the L generated vortices written in vector notation are:

$$\begin{bmatrix} \eta \\ b_{vL} \\ 0 \end{bmatrix} \quad \text{and} \quad \begin{bmatrix} \eta \\ -b_{vL} \\ 0 \end{bmatrix} \quad 0 \leq \eta \leq -\infty$$

The motivation for transformation into the L axes system is this, the key to determining vortex interaction is the distance from the vortex to a point on the trailing wing, and that distance is a function of separation and attitude.

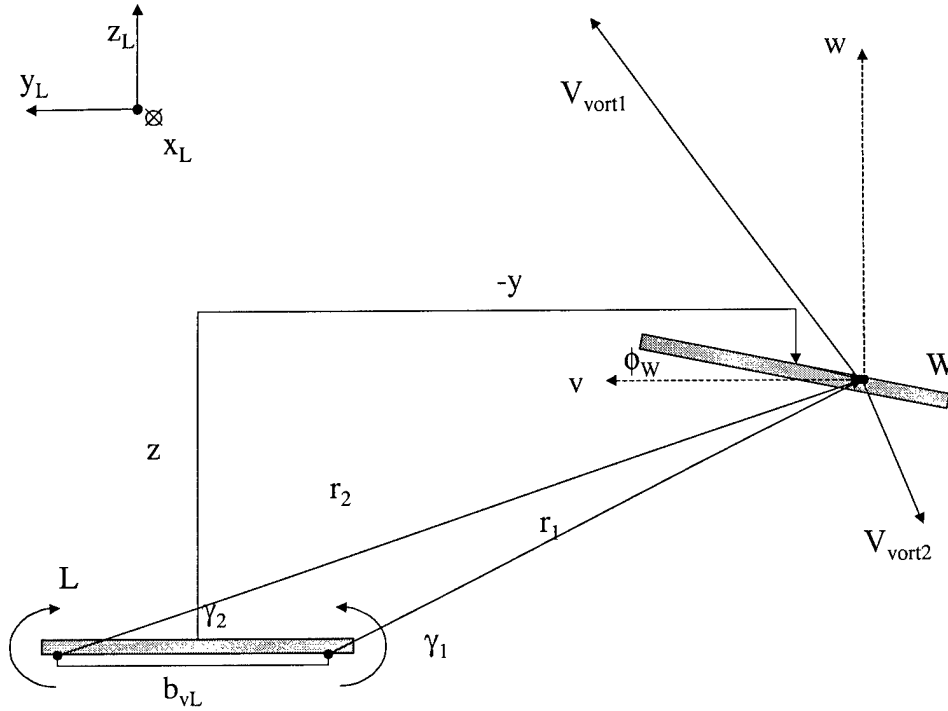


**Figure 5. Separation and Attitude in the L Reference Frame.**

As in [1] and [9], each wing can be represented as a single horseshoe vortex system. Although the assumption of using an elliptically loaded wing to define the vortex separation is rigorously true for pure wings (no fuselage effects) with high aspect ratio and no sweep back, studies conducted by the Air Force's Flight Dynamics Laboratory, [11], indicate that the assumption is approximately true even for modern fighter aircraft. With this assumption, the effective separation of the vortex legs, called  $b_v$ , is  $\pi/4$  times the wing span,  $b$ , of the generating aircraft. The vortex strength, quantified by the circulation,  $\Gamma$ , is

$$\Gamma = \frac{L}{\rho V_{\infty} b_v} = \frac{2V_{\infty} b C_{L_L}}{\pi A R} \quad (3.5.1.1)$$

The vortex flow velocity on aircraft flying in formation is dependent on circulation, the distance from the vortex to the trailing aircraft wing,  $r$ , and the radius of the vortex core,  $r_c$ . The vortex core radius is defined as the distance from the vortex center to the point of maximum velocity and is a function of the kinematic viscosity of the fluid. The Burnham profile for velocity is,

$$V_{vort} = \frac{\Gamma}{2\pi} \left( \frac{r}{r^2 + r_c^2} \right) \quad (3.5.1.2)$$

Applying the superposition principle to the trailing vortices and neglecting the filament attached to the wing of L, the vortex flow velocity is the difference between the flow from the near vortex and the flow from the far vortex. This relationship is illustrated in Figure 5. However, the complication arises in the calculation of  $r_1$  and  $r_2$ , the distance from the vortex filaments to a point on the wing, because now the wing separation and attitude must be expressed in the L reference frame. By using vector addition and axes transformations, all distances are resolved into the L rotating reference frame. Distances from the vortices to a point on the trailing aircraft can be found from geometry.

$$r_1 = \left( \begin{bmatrix} 0 \\ b_{vL} \\ 0 \end{bmatrix} - C_I^L C_w^I \begin{bmatrix} x \\ y \\ z \end{bmatrix} - C_I^L C_w^I \begin{bmatrix} 0 \\ \xi \\ 0 \end{bmatrix} \right) \begin{Bmatrix} \hat{x}_L \\ \hat{y}_L \\ \hat{z}_L \end{Bmatrix} \quad (3.5.1.3)$$

$$r_2 = \left( \begin{bmatrix} 0 \\ -b_{vL} \\ 0 \end{bmatrix} - C_I^L C_w^I \begin{bmatrix} x \\ y \\ z \end{bmatrix} - C_I^L C_w^I \begin{bmatrix} 0 \\ \xi \\ 0 \end{bmatrix} \right) \begin{Bmatrix} \hat{x}_L \\ \hat{y}_L \\ \hat{z}_L \end{Bmatrix}$$

The angle associated with each distance, is the inverse cosine of the y-direction component of the corresponding distance divided by the whole distance. Note that  $\xi$  is the integration variable used to represent the distance along the wing span.

$$\begin{aligned}\theta_1 &= \cos^{-1}\left(\frac{r_1\{\hat{y}_L\}}{r_1}\right) \\ \theta_2 &= \cos^{-1}\left(\frac{r_2\{\hat{y}_L\}}{r_2}\right)\end{aligned}\tag{3.5.1.4}$$

The velocities caused by the vortices can be superposed to give a total average velocity vector in the L rotating reference frame,

$$\begin{bmatrix} u \\ v \\ w \end{bmatrix}_L = \begin{bmatrix} 0 \\ V_{vort1} \sin \theta_1 - V_{vort2} \sin \theta_2 \\ V_{vort1} \cos \theta_1 - V_{vort2} \cos \theta_2 \end{bmatrix} \begin{Bmatrix} \hat{x}_L \\ \hat{y}_L \\ \hat{z}_L \end{Bmatrix}$$

Substituting for the vortex velocities,  $V_{vort}$ , with the Burnham profile expression found in equation (3.5.1.2) and the angle relationships from equation (3.5.1.4) creates,

$$\begin{bmatrix} u \\ v \\ w \end{bmatrix}_L = \begin{bmatrix} 0 \\ \frac{\Gamma}{2\pi} \left( \frac{r_1}{r_1^2 + r_c^2} \right) \left( \frac{r_1\{\hat{z}_L\}}{r_1} \right) - \frac{\Gamma}{2\pi} \left( \frac{r_2}{r_2^2 + r_c^2} \right) \left( \frac{r_2\{\hat{z}_L\}}{r_2} \right) \\ \frac{\Gamma}{2\pi} \left( \frac{r_1}{r_1^2 + r_c^2} \right) \left( \frac{r_1\{\hat{y}_L\}}{r_1} \right) - \frac{\Gamma}{2\pi} \left( \frac{r_2}{r_2^2 + r_c^2} \right) \left( \frac{r_2\{\hat{y}_L\}}{r_2} \right) \end{bmatrix} \begin{Bmatrix} \hat{x}_L \\ \hat{y}_L \\ \hat{z}_L \end{Bmatrix}$$

This can be further modified by substituting the relationship for circulation, canceling appropriate terms, and inserting the applicable distance relationships. The  $x_L$ -component

of distance is set to zero because of the assumption of constant vortex strength of the vortex filament in the  $x_L$ -direction.

$$\begin{bmatrix} u \\ v \\ w \end{bmatrix}_L = \left( \frac{L_L}{2\pi\rho V_\infty b_{vL}} \right) \begin{bmatrix} 0 \\ \left( \frac{r_1(z_L)}{r_1^2 + r_c^2} \right) - \left( \frac{r_2(z_L)}{r_2^2 + r_c^2} \right) \\ \left( \frac{r_1(y_L)}{r_1^2 + r_c^2} \right) - \left( \frac{r_2(y_L)}{r_2^2 + r_c^2} \right) \end{bmatrix} \begin{Bmatrix} \hat{x}_L \\ \hat{y}_L \\ \hat{z}_L \end{Bmatrix} \quad (3.5.1.5)$$

Using the transformation matrices the vortex related velocity vector can be transformed from the L rotating reference frame into W.

$$\begin{bmatrix} u \\ v \\ w \end{bmatrix}_W = C_I^W C_L^I \begin{bmatrix} u \\ v \\ w \end{bmatrix}_L \quad (3.5.1.6)$$

### 3.5.2 Lift and Drag Analysis

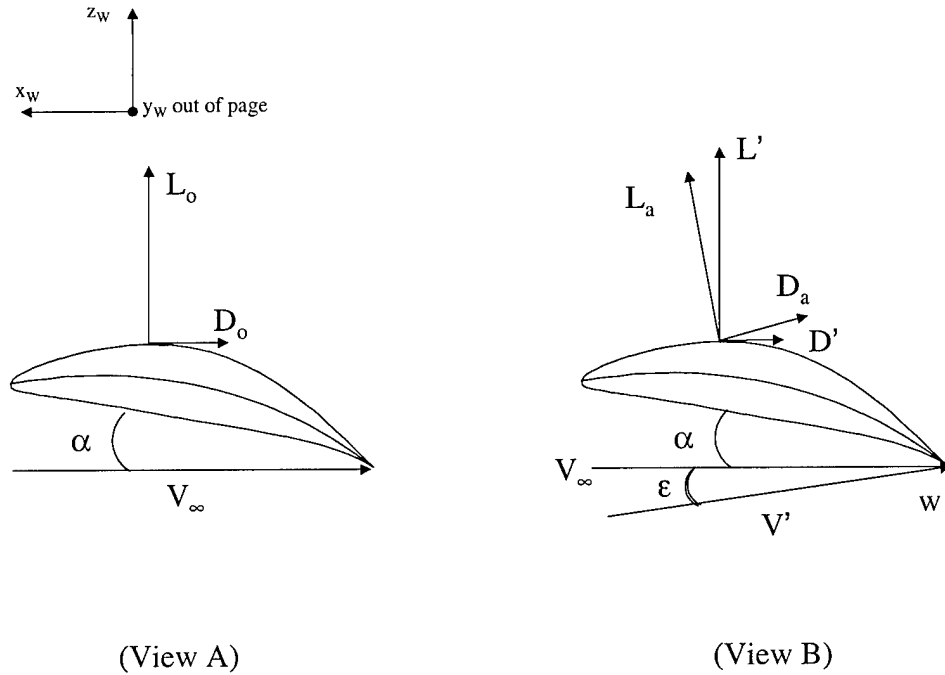


**Figure 6. Lift Vector Rotation on W Wing.**

View A in Figure 6 shows the wing in ordinary flight, meaning a single aircraft with no vortex interaction. View B shows the rotation of the lift vector due to the action of the L vortex filament and the new lift,  $L'$ , in the direction of the original lift vector.  $L'$  and  $D'$  are in the direction of the original lift and drag, but increased and decreased in magnitude, respectively. The reduction of induced drag is the essence of close formation flight. The change in the angle of attack as shown in Figure 6 can be found using trigonometry. The assumption of a small incidence angle,  $\epsilon$ , is substantiated in [15], where the research found  $\epsilon$  ranged from two to four degrees. Applying small angle assumptions, the inverse tangent of a ratio is approximately equal to the ratio.

$$\varepsilon = \tan^{-1}(w/V_{\infty}) \approx w/V_{\infty}$$

The next step is to derive expressions for the change in lift and drag from the original values to the new values. This is done by starting with the definition of lift as being the product of the lift curve slope,  $L_{\alpha}$ , and the angle of attack,  $\alpha$ . The subscript o refers to the original lift or drag.

$$L_o = L_{\alpha} \alpha$$

$$D_o = \left( \frac{D}{L} \right)_o L_o = \left( \frac{D}{L} \right)_o L_{\alpha} \alpha$$

Similarly the rotated lift and drag, subscript a, can be written as,

$$L_a = L_{\alpha} (\alpha + \varepsilon) \tag{3.5.2.1}$$

$$D_a = \left( \frac{D}{L} \right)_a L_a = \left( \frac{D}{L} \right)_a L_{\alpha} (\alpha + \varepsilon)$$

The small angle approximation is also used to simplify the trigonometric expressions for the new lift and drag associated with the flight path direction.

$$L' = L_a \cos \varepsilon + D_a \sin \varepsilon \approx L_a + D_a \varepsilon \tag{3.5.2.2}$$

$$D' = D_a \cos \varepsilon - L_a \sin \varepsilon \approx D_a - L_a \varepsilon$$

Substituting the expressions from equation (3.5.2.1) into the L' equation shown above yields,

$$L' = L_{\alpha} (\alpha + \varepsilon) + \left( \frac{D}{L} \right)_a L_{\alpha} (\alpha + \varepsilon) \varepsilon$$

Multiplying and collecting like terms allows the new lift,  $L'$  to be written as,

$$L' = L_{\alpha}\alpha + L_{\alpha}\left(\varepsilon + \left(\frac{D}{L}\right)\alpha\varepsilon + \left(\frac{D}{L}\right)\varepsilon^2\right)$$

For the small values attributable to  $\varepsilon$ , it is a valid approximation to say that the original drag to lift ratio is equal to the rotated drag to lift ratio, and that the lift curve slope remains constant. The new lift,  $L'$ , can be written in terms of the original lift,  $L_o$ , by making substitutions and neglecting the very small terms.

$$L' \cong L_o + L_{\alpha}\varepsilon$$

Therefore the change in lift resulting from vortex interaction can be written as a function of lift curve slope, freestream velocity, and the upwash velocity,  $w$ .

$$\Delta L = L_{\alpha}\left(\frac{w}{V_{\infty}}\right) \quad (3.5.2.3)$$

A derivation similar to the one for the change in lift can be conducted to find the new drag,  $D'$ . Again the difference between the original drag and the new drag can be found starting with substituting the relationships for  $D_a$  and  $L_a$  from equation (3.5.2.1) into the expression for  $D'$  from (3.5.2.2).

$$D' = \left(\frac{D}{L}\right)L_{\alpha}(\alpha + \varepsilon) - L_{\alpha}(\alpha + \varepsilon)\varepsilon$$

Again multiplying and collecting like terms allows  $D'$  to be written as,

$$D' = \left(\frac{D}{L}\right)L_{\alpha}\alpha - L_{\alpha}\left(\alpha\varepsilon + \varepsilon^2 - \left(\frac{D}{L}\right)\varepsilon\right)$$

As in the new lift derivation, assumptions are made about constant drag to lift ratios and small angles which yield,

$$D' \cong D_o - L_\alpha \alpha \varepsilon$$

As with the change in lift, the change in drag caused by close formation flight can be written as a function of lift curve slope, angle of attack, freestream velocity, and the upwash velocity,  $w$ .

$$\Delta D = -L_\alpha \alpha \left( \frac{w}{V_\infty} \right) \quad (3.5.2.4)$$

It is vital to recognize that the z-component of velocity,  $w$ , used in this derivation is in the W rotating reference frame.

### 3.5.3 *Upwash Velocity Equations*

From equations (3.5.2.3) and (3.5.2.4), the only information remaining to be found in the calculation of the change in lift and drag is the of upwash,  $w$ , across the W wing. This is accomplished by first finding the average velocity vector components in the L frame of reference and then transforming the vector into the W frame. The integration is conducted as though the wing were a lifting line equal in distance to the span between the trailing vortices,  $b_v$ , and is non-dimensionalized by dividing the integrand by  $b_v$ .

$$(\Delta L)_W = \int_{-b_{vW}/2}^{b_{vW}/2} L_\alpha \left( \frac{w}{V_\infty} \right) \left( \frac{dy}{b_{vW}} \right)$$

$$(\Delta D)_W = \int_{-b_{vW}/2}^{b_{vW}/2} -L_\alpha \alpha \left( \frac{w}{V_\infty} \right) \left( \frac{dy}{b_{vW}} \right)$$

By substituting the relationship for  $w$  in the integrand, which is the vortex velocity component in the  $z_W$ -direction, with the velocity expression from equation (3.5.1.6) and removing the constants from the integrand yields the following expressions:

$$(\Delta L)_W = \frac{L_\alpha}{V_\infty b_{vW}} \left( \frac{L_L}{2\pi\rho V_\infty b_{vL}} \right) \begin{bmatrix} 0 \\ 0 \\ 1 \end{bmatrix} C_I^W C_L^I \sigma$$

$$(\Delta D)_W = \frac{-L_\alpha \alpha}{V_\infty b_{vW}} \left( \frac{L_L}{2\pi\rho V_\infty b_{vL}} \right) \begin{bmatrix} 0 \\ 0 \\ 1 \end{bmatrix} C_I^W C_L^I \sigma$$

Where the function  $\sigma$  is defined as,

$$\sigma = \begin{bmatrix} \int_{-b_{vW}/2}^{b_{vW}/2} \left( \frac{r_1 \{\hat{z}_L\}}{r_1^2 + r_c^2} \right) - \left( \frac{r_2 \{\hat{z}_L\}}{r_2^2 + r_c^2} \right) d\xi \\ \int_{-b_{vW}/2}^{b_{vW}/2} \left( \frac{r_1 \{\hat{y}_L\}}{r_1^2 + r_c^2} \right) - \left( \frac{r_2 \{\hat{y}_L\}}{r_2^2 + r_c^2} \right) d\xi \end{bmatrix} \begin{Bmatrix} \hat{x}_L \\ \hat{y}_L \\ \hat{z}_L \end{Bmatrix}$$

with the expressions for  $r_1$  and  $r_2$  found in equation (3.5.1.3). Integrating and collecting terms yields,

$$\sigma(x_L) = 0 \quad (3.5.3.1)$$

$$\begin{aligned} \sigma(y_L) = & \frac{-z}{\sqrt{C^2 x^2 + C^2 z^2 + r_c^2}} \left[ a \tan \left( \frac{b_v C - b_v + 2Cy}{2\sqrt{C^2 x^2 + C^2 z^2 + r_c^2}} \right) - \right. \\ & a \tan \left( \frac{b_v C + b_v + 2Cy}{2\sqrt{C^2 x^2 + C^2 z^2 + r_c^2}} \right) - a \tan \left( \frac{-b_v C - b_v + 2Cy}{2\sqrt{C^2 x^2 + C^2 z^2 + r_c^2}} \right) + \\ & \left. a \tan \left( \frac{-b_v C + b_v + 2Cy}{2\sqrt{C^2 x^2 + C^2 z^2 + r_c^2}} \right) \right] \end{aligned} \quad (3.5.3.2)$$

$$\begin{aligned} \sigma(z_L) = & -\frac{1}{2C} \ln \left[ \left( \frac{b_v(1+2C+C^2)+4Cb_v y(1+C)+4C^2(x^2+y^2+z^2)+4r_c^2}{b_v(1-2C+C^2)+4Cb_v y(-1+C)+4C^2(x^2+y^2+z^2)+4r_c^2} \right)^* \right. \\ & \left. \left( \frac{b_v(1+2C+C^2)+4Cb_v y(-1-C)+4C^2(x^2+y^2+z^2)+4r_c^2}{b_v(1-2C+C^2)+4Cb_v y(-1+C)+4C^2(x^2+y^2+z^2)+4r_c^2} \right) \right] \end{aligned} \quad (3.5.3.3)$$

where C is short hand for the coordinate transformation,

$$C \equiv C_I^L C_W^I$$

Note that when the two rotating reference frames are aligned, these three equations are mathematically equal to the ones found in both [8] and [10].

#### 3.5.4 Vortex Effects on the Vertical Tail

Recalling the requirement to fly with no sideslip, the only side force,  $Y_W$ , on the vertical tail of the wing aircraft is caused by the component of vortex flow in the y-direction of the W rotating reference frame. The analysis for the side force follows the same steps as wing analysis, the primary difference coming in the distance vector calculation.

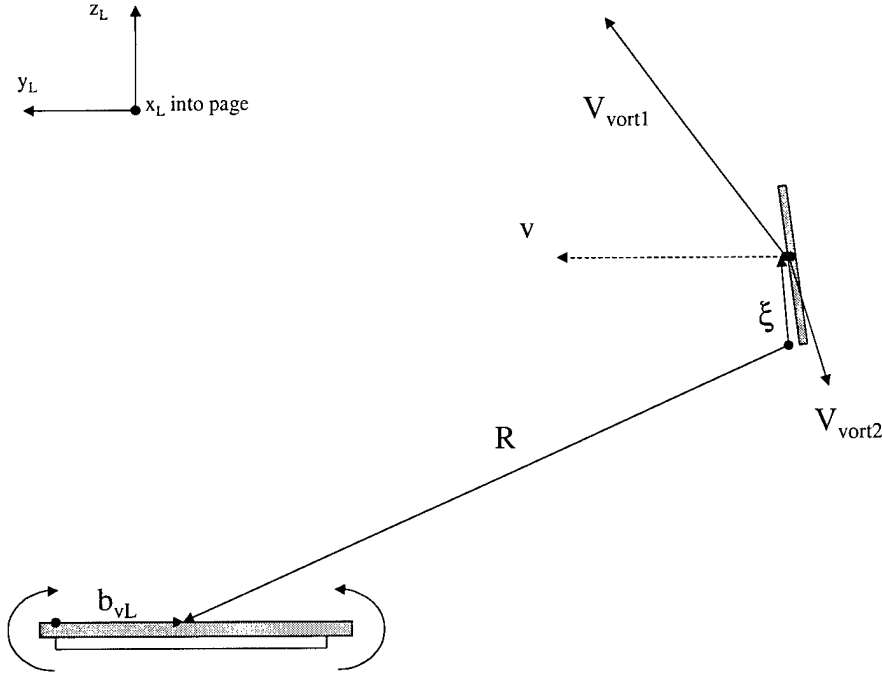


**Figure 7. Vertical Tail of W in Vortex Interaction.**

As shown in Figure 7, the distance from the vortices to a location on the vertical tail can be written as vectors in the associated rotating reference frame, which can then be transformed so all distances are in the L frame. The only difference between the wing and vertical tail separation is the integration variable,  $\xi$ , that now is in the  $z$  direction of the W reference frame.

$$r_{1vt} = \left( \begin{bmatrix} 0 \\ b_{vL} \\ 0 \end{bmatrix} - C_I^L C_W^I \begin{bmatrix} x \\ y \\ z \end{bmatrix} - C_I^L C_W^I \begin{bmatrix} 0 \\ 0 \\ \xi \end{bmatrix} \right) \begin{Bmatrix} \hat{x}_L \\ \hat{y}_L \\ \hat{z}_L \end{Bmatrix} \quad (3.5.4.1)$$

$$r_{2vt} = \left( \begin{bmatrix} 0 \\ -b_{vL} \\ 0 \end{bmatrix} - C_I^L C_W^I \begin{bmatrix} x \\ y \\ z \end{bmatrix} - C_I^L C_W^I \begin{bmatrix} 0 \\ 0 \\ \xi \end{bmatrix} \right) \begin{Bmatrix} \hat{x}_L \\ \hat{y}_L \\ \hat{z}_L \end{Bmatrix}$$

The force and drag analysis on the vertical tail follows a similar pattern as for the wing with all the same assumptions and conditions, except that the initial angle of attack is zero. The change in side force is the parameter of interest and has the same result as the change in lift on the wing. Figure 8 shows the velocity vectors and forces on the vertical tail.

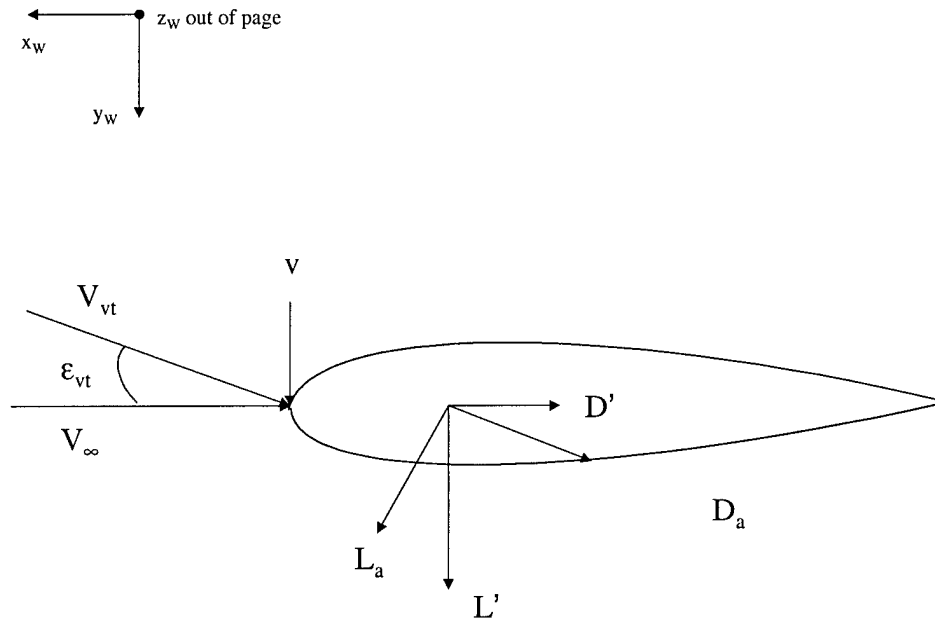


**Figure 8. Interaction Forces on the Vertical Tail (viewed from above).**

The change in side force on the vertical tail,  $\Delta Y$ , can be written,

$$\Delta Y = L_{\alpha_{vt}} \epsilon_{vt}$$

Again, the form of the vortex interaction equation remains the same as for the wing, with the function  $\sigma_{vt}$  and lift curve slope being subscripted to reflect the vertical tail values, as opposed to those of the wing.

$$(\Delta Y)_W = \frac{L_{vt\alpha}}{V_\infty b_{vt}} \left( \frac{L_L}{2\pi\rho V_\infty b_{vL}} \right) \begin{bmatrix} 0 \\ 0 \\ 1 \end{bmatrix} C_I^W C_L^I \sigma_{vt}$$

Where  $\sigma_{vt}$  is defined as,

$$\sigma_{vt} = \begin{bmatrix} \int_0^{b_{vt}} \left( \frac{r_{1vt} \{\hat{z}_L\}}{r_{1vt}^2 + r_c^2} \right) - \left( \frac{r_{2vt} \{\hat{z}_L\}}{r_{2vt}^2 + r_c^2} \right) d\xi \\ \int_0^{b_{vt}} \left( \frac{r_{1vt} \{\hat{y}_L\}}{r_{1vt}^2 + r_c^2} \right) - \left( \frac{r_{2vt} \{\hat{y}_L\}}{r_{2vt}^2 + r_c^2} \right) d\xi \\ 0 \end{bmatrix} \begin{Bmatrix} \hat{x}_L \\ \hat{y}_L \\ \hat{z}_L \end{Bmatrix}$$

The limits of the integration are from zero, the longitudinal centerline of W, to  $b_{vt}$ , the height of the vertical tail. The results of the integration are,

$$\sigma(x_L) = 0 \quad (3.5.4.2)$$

$$\begin{aligned} \sigma(y_L) = & \frac{2y}{\sqrt{4C^2 x^2 + (2Cy - b_{vL})^2 + 4r_c^2}} \left[ a \tan \left( \frac{2Cz}{\sqrt{4C^2 x^2 + (2Cy - b_{vL})^2 + 4r_c^2}} \right) - \right. \\ & \left. a \tan \left( \frac{2C(b_{vt} + z)}{\sqrt{4C^2 x^2 + (2Cy - b_{vL})^2 + 4r_c^2}} \right) \right] + \\ & \frac{2y}{\sqrt{4C^2 x^2 + (2Cy + b_{vL})^2 + 4r_c^2}} \left[ a \tan \left( \frac{2Cz}{\sqrt{4C^2 x^2 + (2Cy + b_{vL})^2 + 4r_c^2}} \right) - \right. \\ & \left. a \tan \left( \frac{2C(-b_{vt} + z)}{\sqrt{4C^2 x^2 + (2Cy + b_{vL})^2 + 4r_c^2}} \right) \right] \end{aligned} \quad (3.5.4.3)$$

$$\sigma(z_L) = -\frac{1}{2C} \ln \left( \frac{(2Cy + b_{vL})^2 + 4C^2(x^2 + (b_{vt} + z)^2) + 4r_c^2}{(2Cy - b_{vL})^2 + 4C^2(x^2 + (b_{vt} + z)^2) + 4r_c^2} \right) +$$

$$\ln \left( \frac{(2Cy - b_{vL})^2 + 4C^2(x^2 + z^2) + 4r_c^2}{(2Cy + b_{vL})^2 + 4C^2(x^2 + z^2) + 4r_c^2} \right) \quad (3.5.4.4)$$

## 4 Formation Flight Controller

### 4.1 Controller Design

The foundation for the controller design is the PID control action on each of the three control channels. For the primary control law thrust control is affected in the x channel, which is to say that any error in the commanded and the actual value of x separation distance, results in a change in thrust. In a similar manner, lift is the control variable in the z channel and roll rate is the control variable in the y channel. Eqs. (4.1.1) – (4.1.3) show the actual control law used for each of the three control variables:  $T_w$ ,  $L_w$ , and  $p_w$ , respectively. Note that the dynamics associated with lateral maneuvers required the inclusion of a second derivative on separation error and proportional feedback of the heading error for the roll rate control variable.

$$T_w = K_{T_P} e_x + K_{T_D} \dot{e}_x + K_{T_I} \int e_x dt \quad (4.1.1)$$

$$L_w = K_{L_P} e_z + K_{L_D} \dot{e}_z + K_{L_I} \int e_z dt \quad (4.1.2)$$

$$p_w = K_{p_P} e_y + K_{\psi_{eP}} e_{\psi_e} + K_{p_D} \dot{e}_y + K_{p_{DD}} \ddot{e}_y + K_{p_I} \int e_y dt \quad (4.1.3)$$

Where the error signals are the difference between the commanded and actual formation geometry separation distances.

$$\begin{bmatrix} e_x \\ e_y \\ e_z \end{bmatrix} = \begin{bmatrix} x_c - x \\ y_c - y \\ z_c - z \end{bmatrix} \quad (4.1.4)$$

The integrals of the error signals are created by augmenting the formation equations of motion. The derivative control elements are created by taking the difference in the separation distances for a single time step and dividing by the magnitude of the time step. As noted above, control in the lateral channel required additional control elements in the control law.

In an attempt to more closely approximate actual pilot control inputs, an alternative control law was devised. For this new control law, the need for W to climb, according to a separation error in the x direction, results in the controller responding with increased thrust, whereas the need for W to increase flight speed causes the lift to decrease. In other words, thrust is now the control variable in the z channel and lift is the control variable in the x channel. Roll rate continues as the control variable in the y channel. Another attempt to simulate the "seat of the pants" feedback used by pilots is the inclusion of acceleration feedback in the alternative control law. Equations for the new control law are shown below.

$$T_w = K_{T_P} e_z + K_{T_D} \dot{e}_z + K_{T_{DD}} \ddot{e}_z + K_{T_I} \int e_z dt \quad (4.1.5)$$

$$L_w = K_{L_P} e_x + K_{L_D} \dot{e}_x + K_{L_{DD}} \ddot{e}_x + K_{L_I} \int e_x dt \quad (4.1.6)$$

$$p_w = K_{P_P} e_y + K_{P_{\psi}} e_{\psi} + K_{P_D} \dot{e}_y + K_{P_{DD}} \ddot{e}_y + K_{P_I} \int e_y dt \quad (4.1.7)$$

In the expressions for the control law above,  $p_w$  is called the roll rate control variable. The actual roll rate,  $P_w$ , can be modified from what is shown in equation (3.2.6), by virtue of a dynamic inversion argument, to be written as,

$$P_w = K_{p_P} e_y + K_{\psi_{e_P}} e_{\psi_e} + K_{p_D} \dot{e}_y + K_{p_{DD}} \ddot{e}_y + K_{p_I} \int e_y dt + \frac{\tan \gamma_w (L_w \sin \phi_w - Y_w \cos \phi_w)}{m_w V_w}$$

## 4.2 Formation Flight Turns

The formation flight control system is such that right and left turns have dissimilar dynamics, dependent upon W's position. This is similar to running on a track, where the runner on the inside lane has to turn sharper (on a shorter path) to stay in his lane. Moreover, pilots fly three different formations during turns. In the first type of formation turn, L remains in W's x-y plane. This is the method used for the design of the automatic formation flight control system. In a "wingtip" formation, W remains in L's x-y plane throughout the turn. In this case, the error signals in Eq. (4.1.4) are transformed into the inertial frame of reference according to

$$\begin{bmatrix} e_x \\ e_y \\ e_z \end{bmatrix} = C_W \begin{bmatrix} x_c - x \\ y_c - y \\ z_c - z \end{bmatrix}$$

prior to the application of the PID control law (Eqs. (4.1.1) – (4.1.3)). In the third mode, called a "route" formation, W and L remain at the same inertial x-y plane during the turn. This type of formation would be accomplished in the simulation by transforming the error signals in Eq. (4.1.4) into the L reference frame according to

$$\begin{bmatrix} e_x \\ e_y \\ e_z \end{bmatrix} = -C_L^T C_W \begin{bmatrix} x_c - x \\ y_c - y \\ z_c - z \end{bmatrix}$$

again prior to the application of the PID control law.

## 5 Formation Flight Simulation Results

### 5.1 Simulation Aircraft

The formation flight control system response to maneuvers flown by the leader and to commanded changes in formation geometry ( $x_c$ ,  $y_c$ , and  $z_c$ ) was simulated using the equations of motion for the two aircraft system shown in equations (3.4.2) – (3.4.8). Both aircraft used in the formation flight simulations were representative of F-16 class aircraft. In the simulations, the formation is flying at an altitude of 15,000 meters and at an airspeed of 0.85 Mach, or approximately 251.5 meters per second. The simulations were conducted with the assumption of incompressible flow. Assumptions were made as to the values of the constants in the drag polar equation (shown in Table 1) in order to determine the thrust required for steady level flight. Naturally, the lift balanced the weight during trimmed flight. The following table shows the aircraft characteristics, obtained from [8], used in the simulations.

**Table 1 F-16 Class Aircraft Specifications**

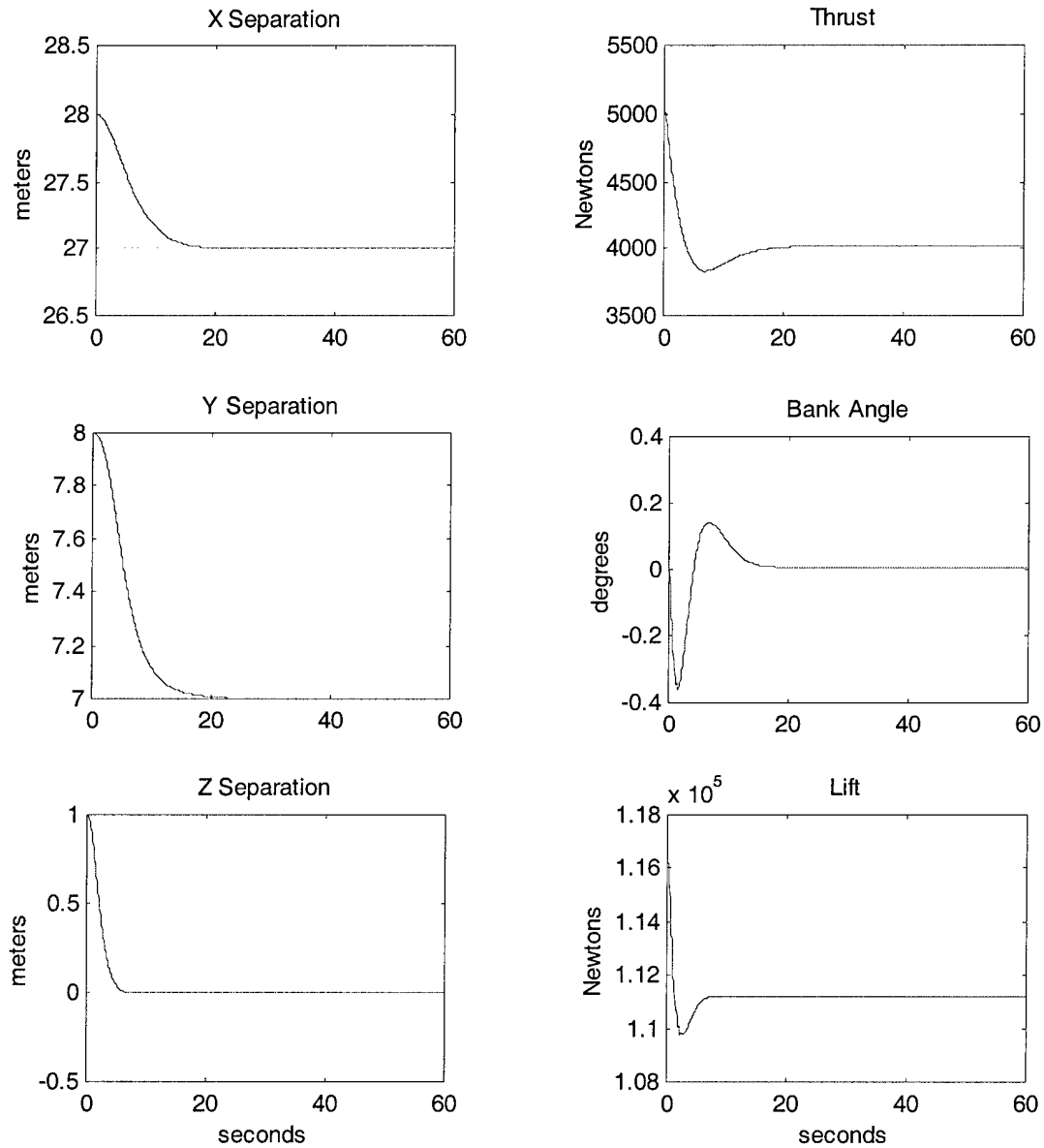
Wing Area	S	27.87 m <sup>2</sup>
Wing Span	b	9.14 m
Aspect Ratio	AR	3
Lift Curve Slope	$L_\alpha$	5.3 per rad
Coefficient of Zero-Lift Drag	$C_{D0}$	0.015
Drag Polar Constant	K	0.02
Tail Area	$S_{vt}$	5.086 m <sup>2</sup>
Tail Height	$b_{vt}$	3.05 m
Tail Lift Curve Slope	$L_{vt\alpha}$	5.3 per rad
Efficiency Factor	$\eta$	0.95
Mass	m	11336.4 m

Given the wing span annotated in Table 1 and referring to the formation geometry discussion in Section 2.2.3, the formation geometry used in the simulations, measured in the W reference frame, was  $x_c = 27$  meters,  $z_c = 0$  meters, and  $y_c = 7$  meters.

## **5.2 Displacement Recovery Maneuvers**

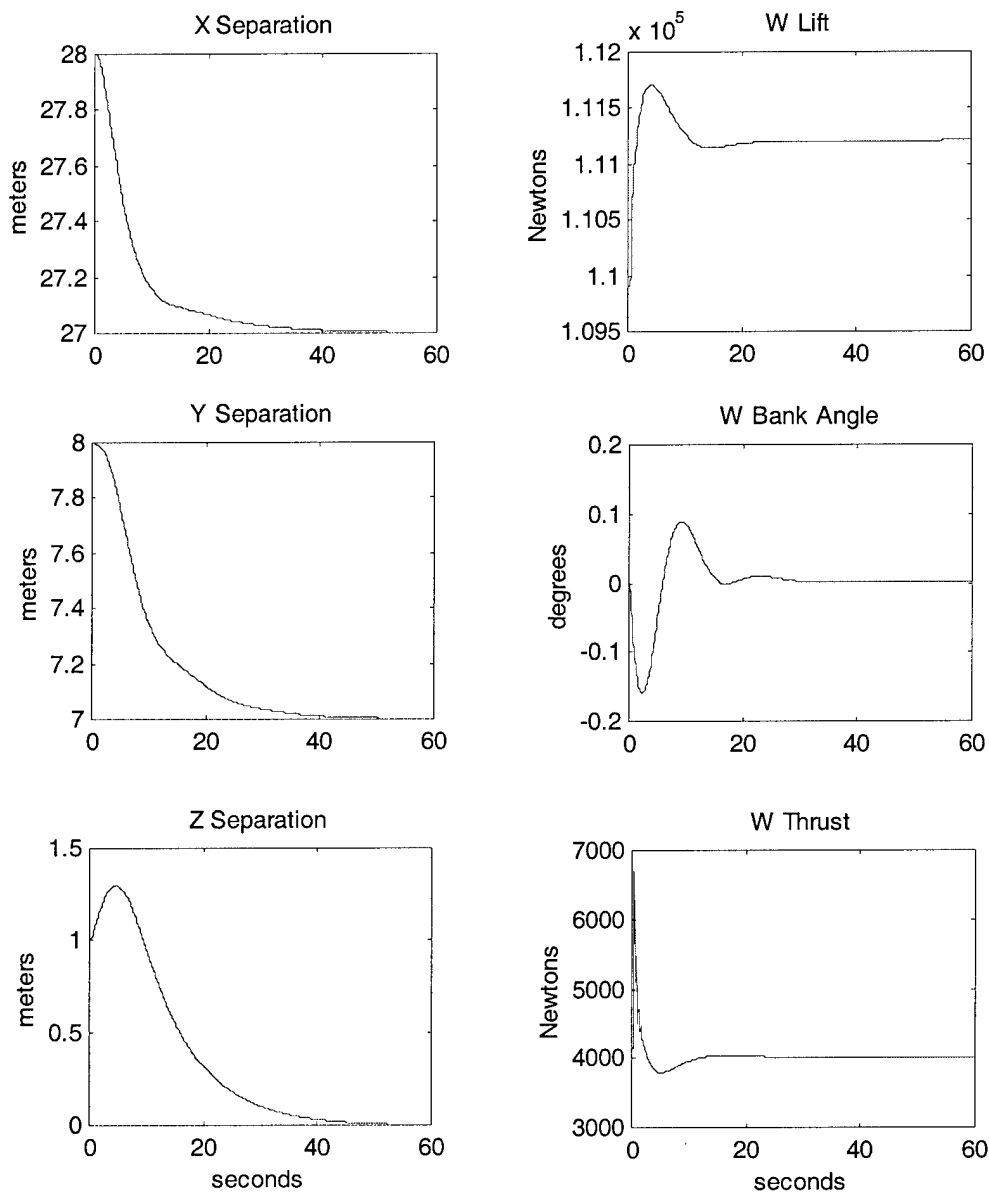
Initially the formation flight control system was exercised by commanding W to perform a repositioning after being displaced by one meter in each of the three Cartesian axes directions. The control system gains were selected to ensure the aircraft would properly return to the commanded position. The simulation results of the control system performance are shown by way of time histories for each maneuver. For several maneuvers, the alternative control system response is also shown for comparative purposes.

Figure 9 displays the control system response to a one meter step input ( $x = x_c+1$ ,  $y = y_c+1$ , and  $z = z_c+1$ ) to the separation distances.



**Figure 9.** W displaced from the optimal position.

In Figure 10, the alternative control law was used to reposition W under the same initial conditions as in the previous figure. Comparing the two system responses, the alternative control law takes longer to recover and has larger control inputs.



**Figure 10. W displaced from optimal position: alternate control law**

In Figure 11, the one meter step input has been changed ( $x = x_c - 1$ ,  $y = y_c - 1$ , and  $z = z_c - 1$ ) to ensure the control system is versatile enough to reposition from a different initial displacement. Again the controller restored  $W$  to the correct formation position.

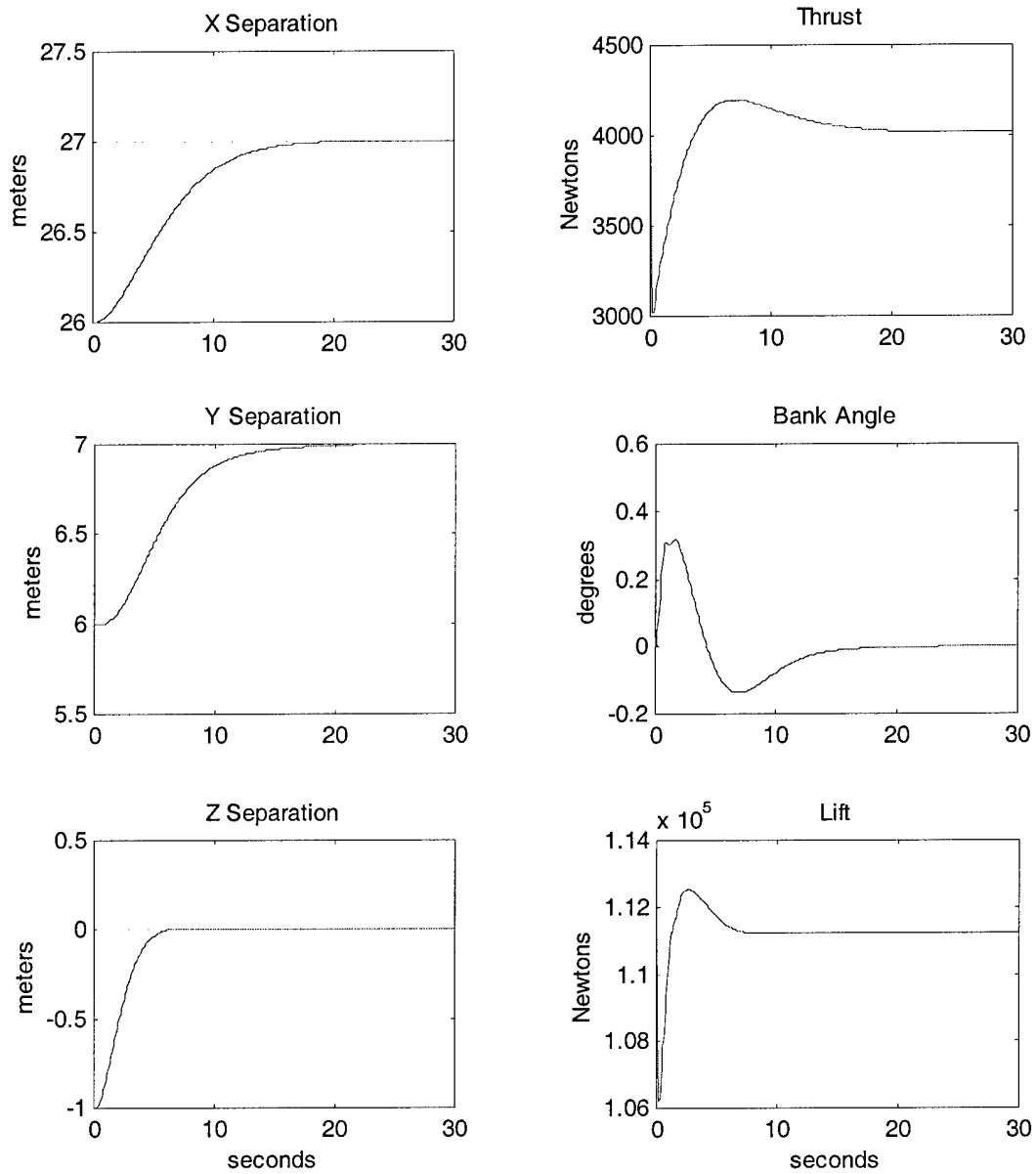


**Figure 11.**  $W$  displaced away from the optimal position.

Because of symmetry, the formation can be aligned on either the right or left wing of the leader. In the formation flight control system, this is accomplished by simply changing the sign on the formation geometry value of commanded y separation,  $y_c$ . For this simulation positive seven became negative seven and W was displaced from this new commanded formation position. The controller response shown in Figure 12 is evidence that the formation can be located on either side of L.

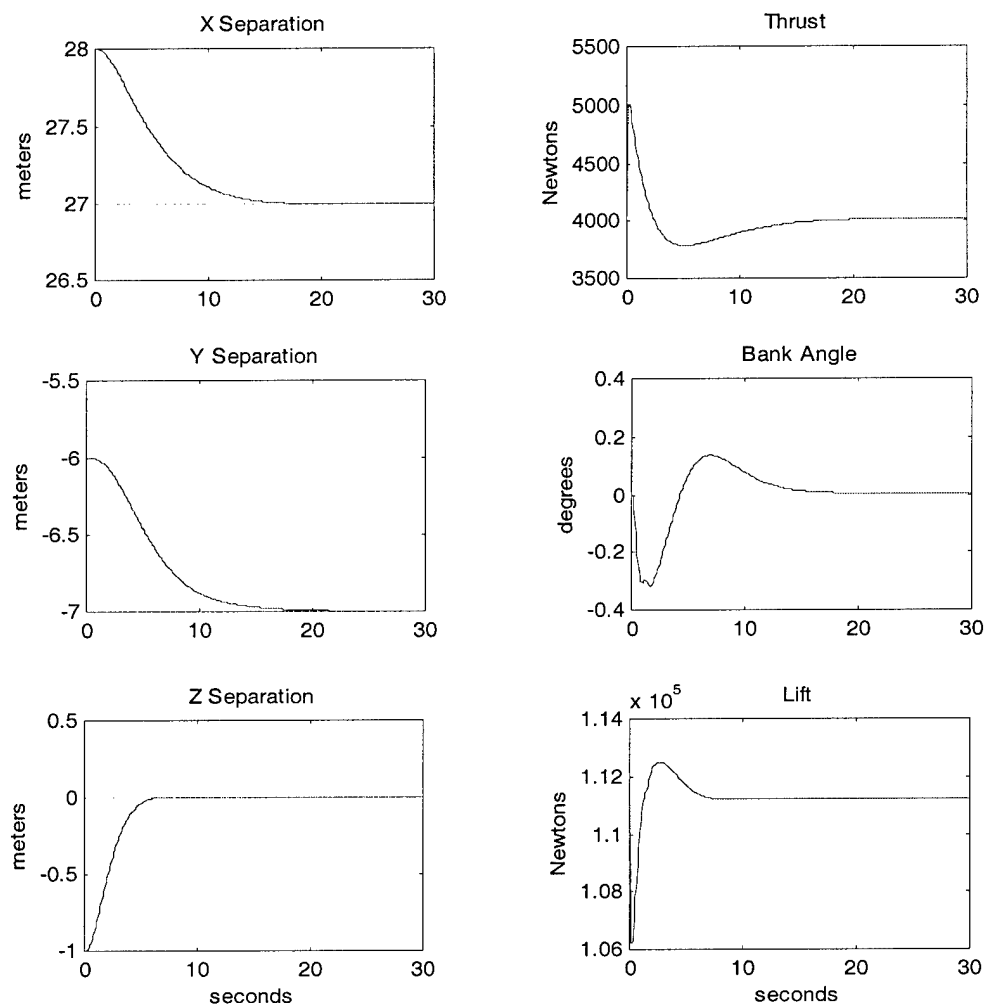
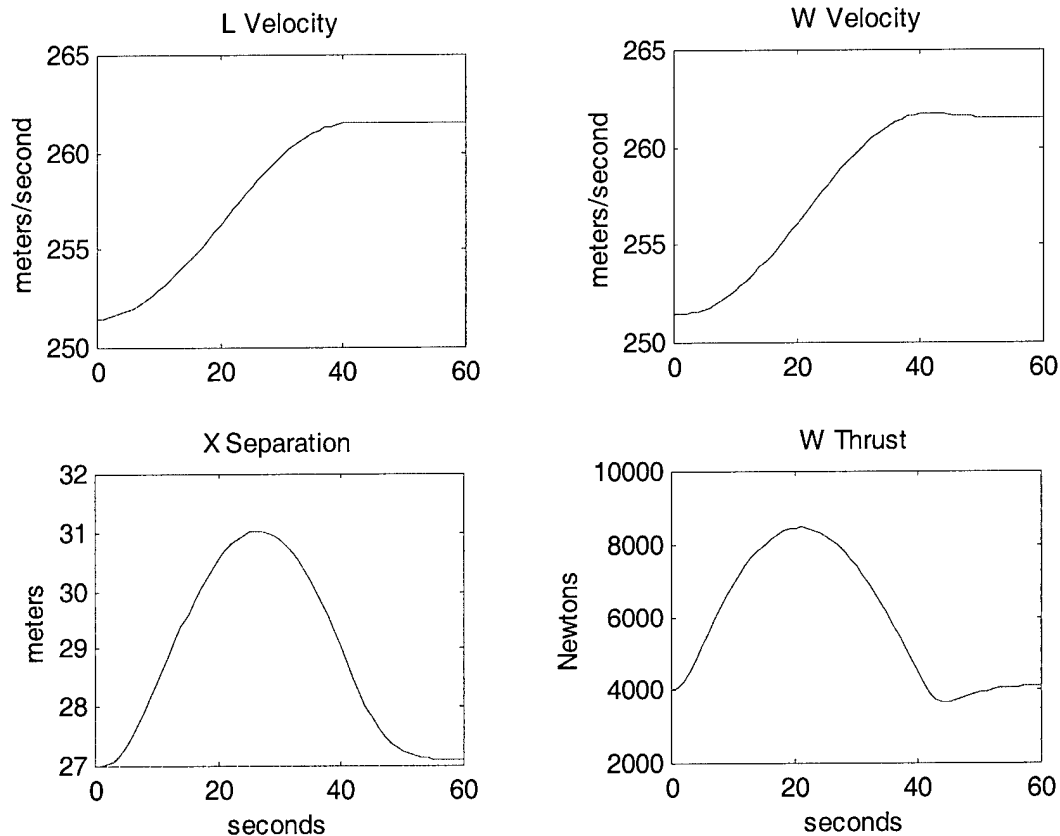


**Figure 12. W displaced from the new optimal position.**

### 5.3 Velocity Change Maneuvers

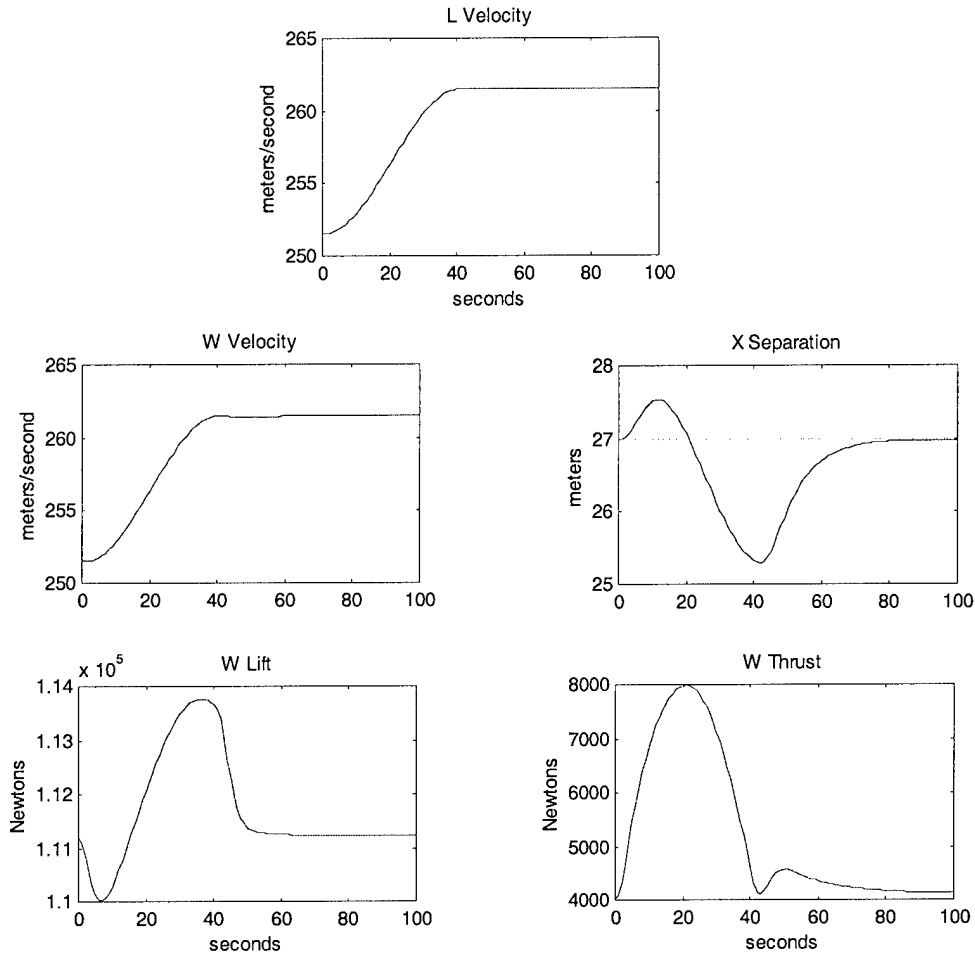
The next step was to fly L through several maneuvers and adjust the gains to the levels required to maintain the formation. Three different maneuvers were explored: L accelerating to a new velocity, L changing altitude, and L changing heading. It is important to note that the requirement of no sideslip mandates that all heading changes be accomplished by rolling the aircraft. While rolling the aircraft, altitude and velocity are maintained by adjusting lift and thrust. In other words, making the heading change is a kinematically coupled maneuver, where adjustments to any control channel affects the other channels. Many trials were made to find suitable gains to accomplish the heading change maneuver. These gains were then reapplied to the other maneuvers to ensure the system would still be able to recover the formation geometry. The first simulations, see Figure 9 - Figure 12, involved L flying straight and level and W recovering from an initial displacement. The next series of simulation results have the leader fly various maneuvers that could be expected during a normal flight. The simplest of these maneuvers was a change in velocity, both positive and negative.

Figure 13 shows how W responded when L's velocity was increased by 10 meters per second. The velocity lag in W is minimal, and the thrust increases in conjunction with the x separation distance and settles at a new steady state value which is slightly greater than the original trim point, as expected.



**Figure 13. W's response to L velocity increase maneuver.**

For comparison purposes, the velocity increase maneuver is repeated using the alternate control law. Again, the indirect nature of the alternative control law causes the second controller to respond differently to system disturbances. In particular, note in Figure 14 the difference in the x separation time histories and the significant amount of lift adjustment made by the second controller when changing velocity, whereas for the primary control system, the change in lift during the velocity change maneuver was almost negligible.



**Figure 14. W's response to L velocity increase maneuver: alternate control law.**

In the next velocity change maneuver, shown in Figure 15, L decreased airspeed and the automatic controller maintained the formation. Note that the value of peak thrust is actually negative. If the model were of a large transport airplane, this could be thought of as engine thrust reversing, but for an F-16, negative thrust would come from the increased drag of air brakes being deployed as the throttles were pulled back.

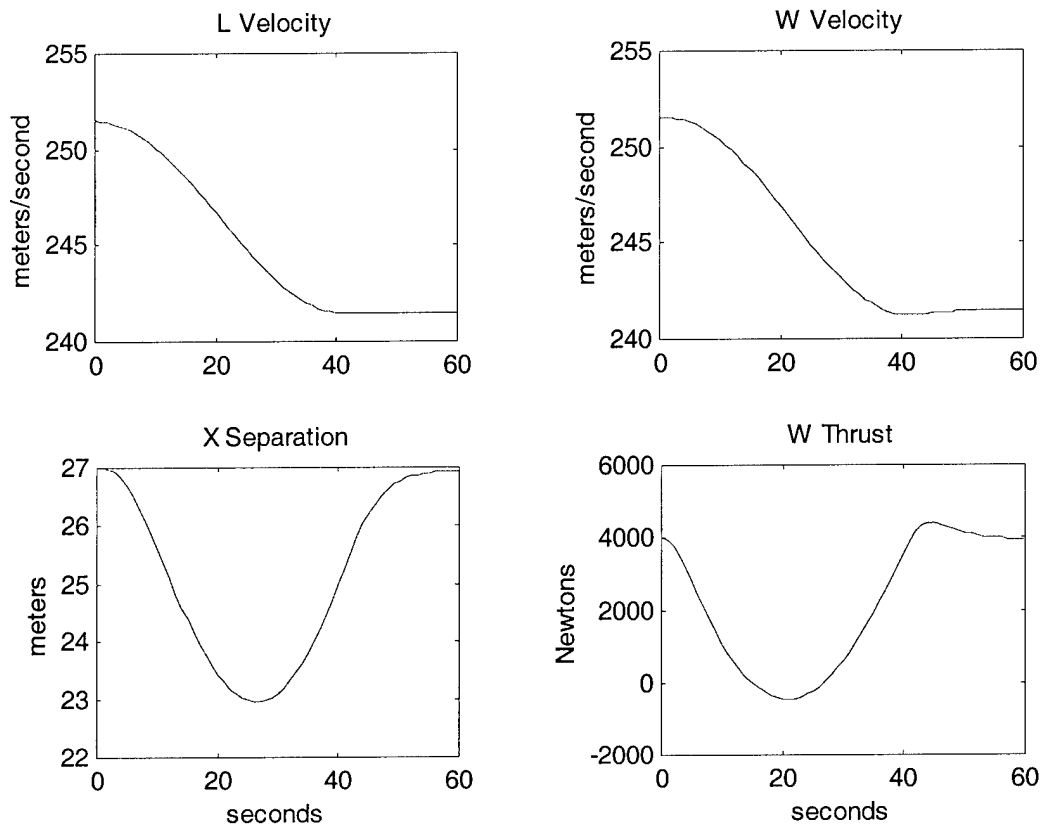


**Figure 15. W's response to L velocity decrease maneuver.**

## 5.4 Altitude Change Maneuvers

Another pitch plane maneuver is the formation altitude increase. In the figure below, the pitch angle of W changes from zero degrees to negative five degrees and back to zero as W climbs to the new altitude. This is due to the definition of positive pitch angle in the wind axes system, as illustrated in Figure 3. L is flown at a constant velocity, which causes the control system to increase W's thrust to maintain proper x separation throughout the climbing portion of the maneuver.

Note in Figure 16 that the z separation shows the control system lag as W adjusts to the leader climbing and then leveling at the new altitude.

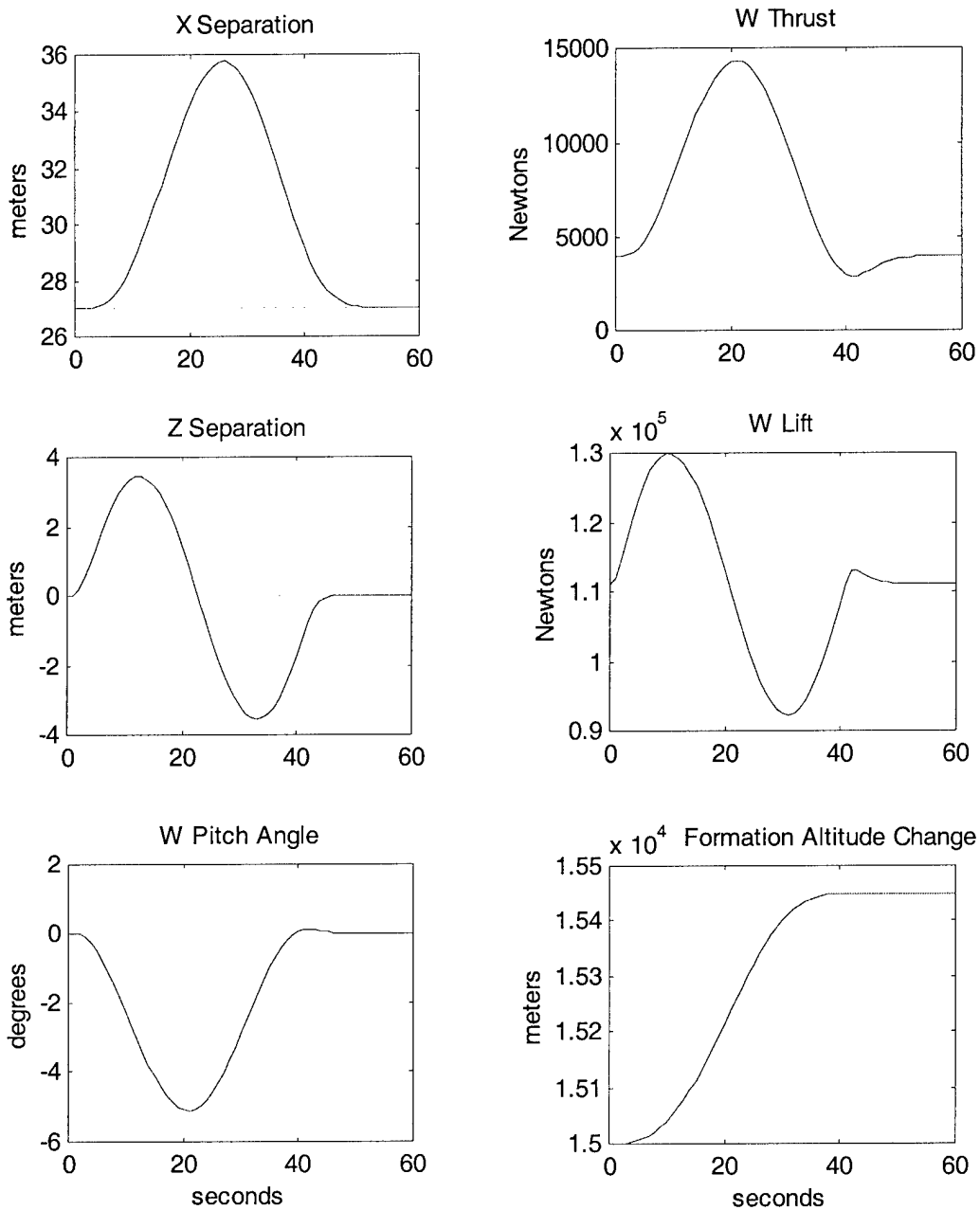


**Figure 16. W's response to L altitude increase maneuver.**

To compare the second controller to the one of primary interest, the altitude increase maneuver was repeated. Note in the figure below that the peak values of thrust and lift are nearly identical to those of the primary control law. However, the transients in the separation distances are dramatically larger using the second controller.

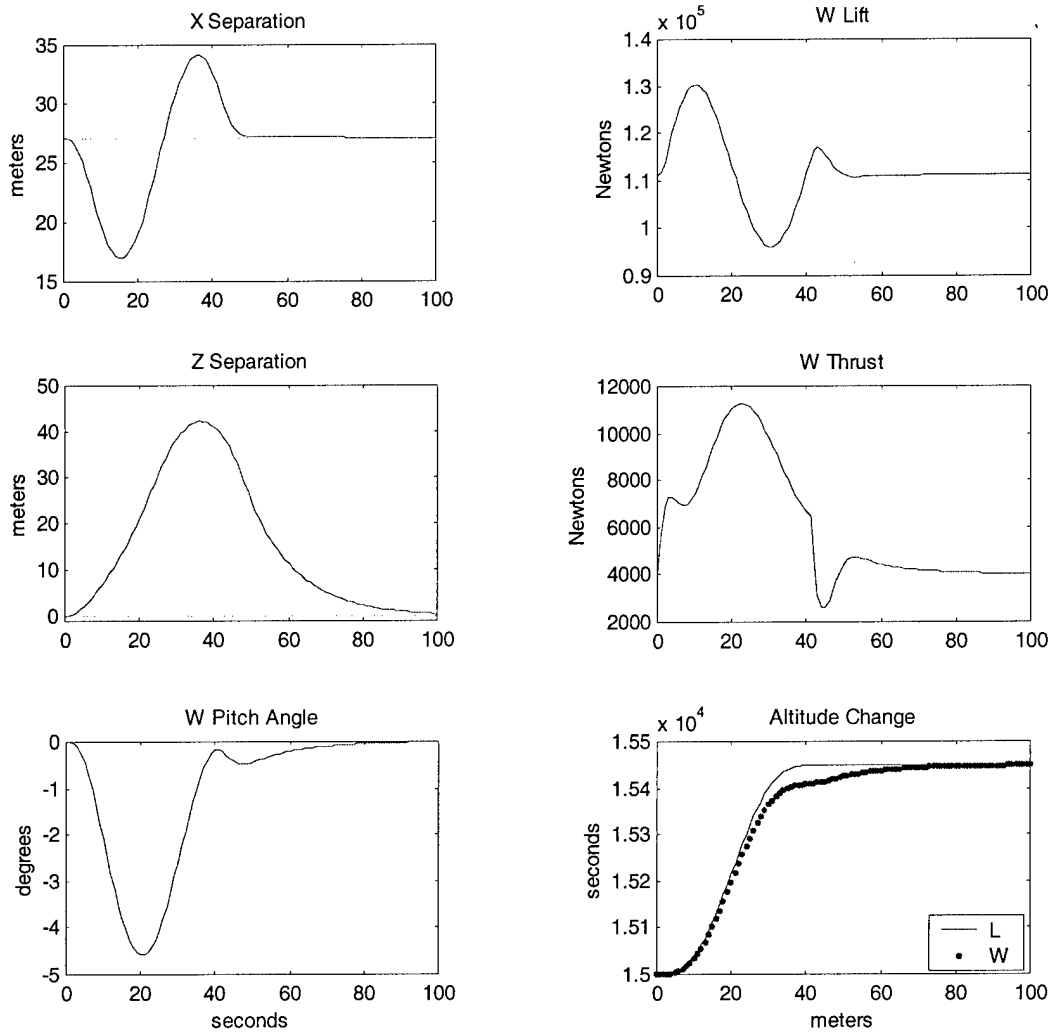


**Figure 17. W's response to L altitude increase maneuver: alternate control law.**

The controller time histories shown in Figure 18 display the control system taking W to a lower altitude in response to L descending. Note that for this maneuver, thrust becomes negative, similar to the velocity decrease maneuver.

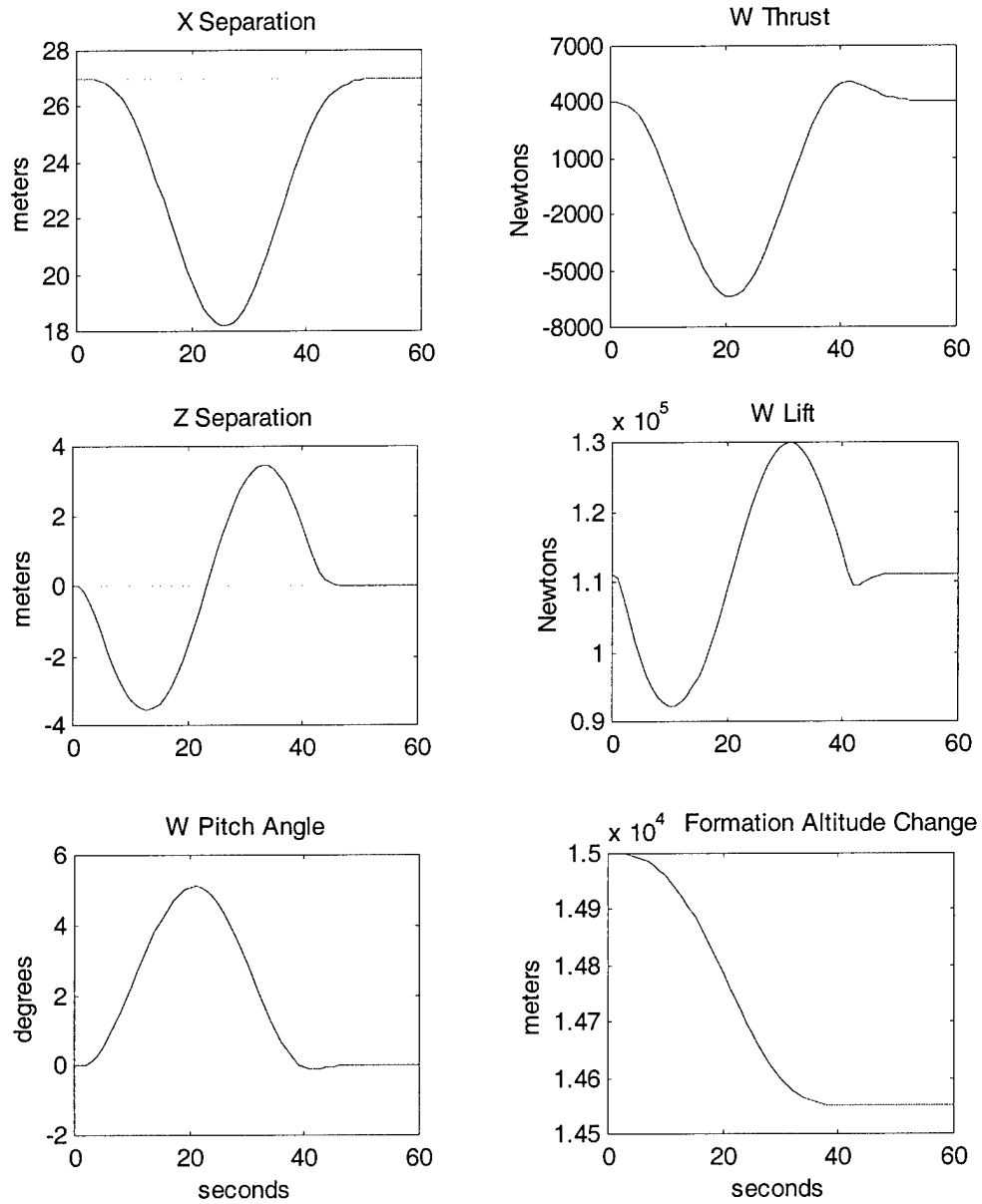


**Figure 18. W's response to L altitude decrease maneuver.**

## 5.5 Heading Change Maneuvers

The kinematic coupling that occurs during turns causes the heading change maneuvers to be more complex for the system to control. The first turning maneuver L conducted was a positive heading change while maintaining constant altitude and velocity. Due to the definition of the wind axes system (Figure 3), a positive heading change is produced by turning to the left. In this maneuver, the formation geometry has W positioned to the right of L, and therefore turning along a wider track. Figure 19 shows roll angle and lift of L as it makes the heading change.

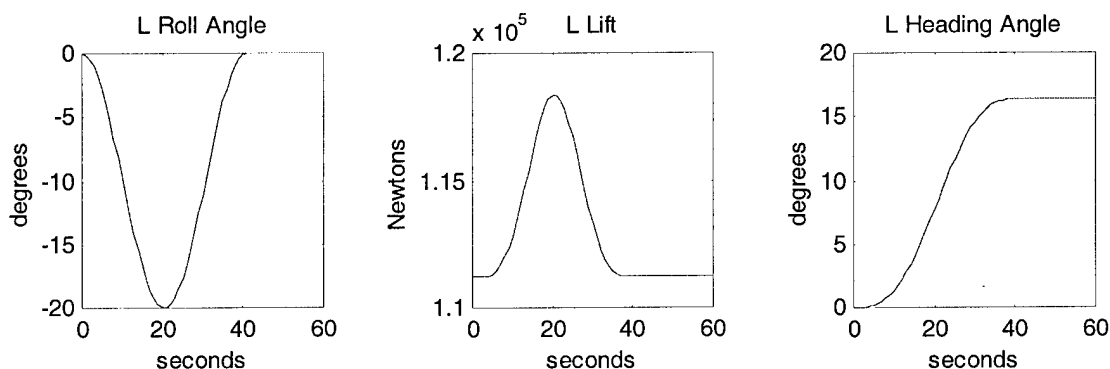


**Figure 19. L positive heading change maneuver.**

The next series of figures show the results of W's control system responses on its position and attitude relative to L. The separation distances measured in the inertial reference frame have been included to show the differences that occurred during this maneuver. For each control channel, the alternate controller response to the same disturbance signal is shown.

The velocity increase in Figure 20 shows the effect of the larger turn radius flown by W. In order to maintain the formation W has to travel at a greater velocity. Note the difference in the final value of the inertial separation distance compared to the W reference frame separation distance.

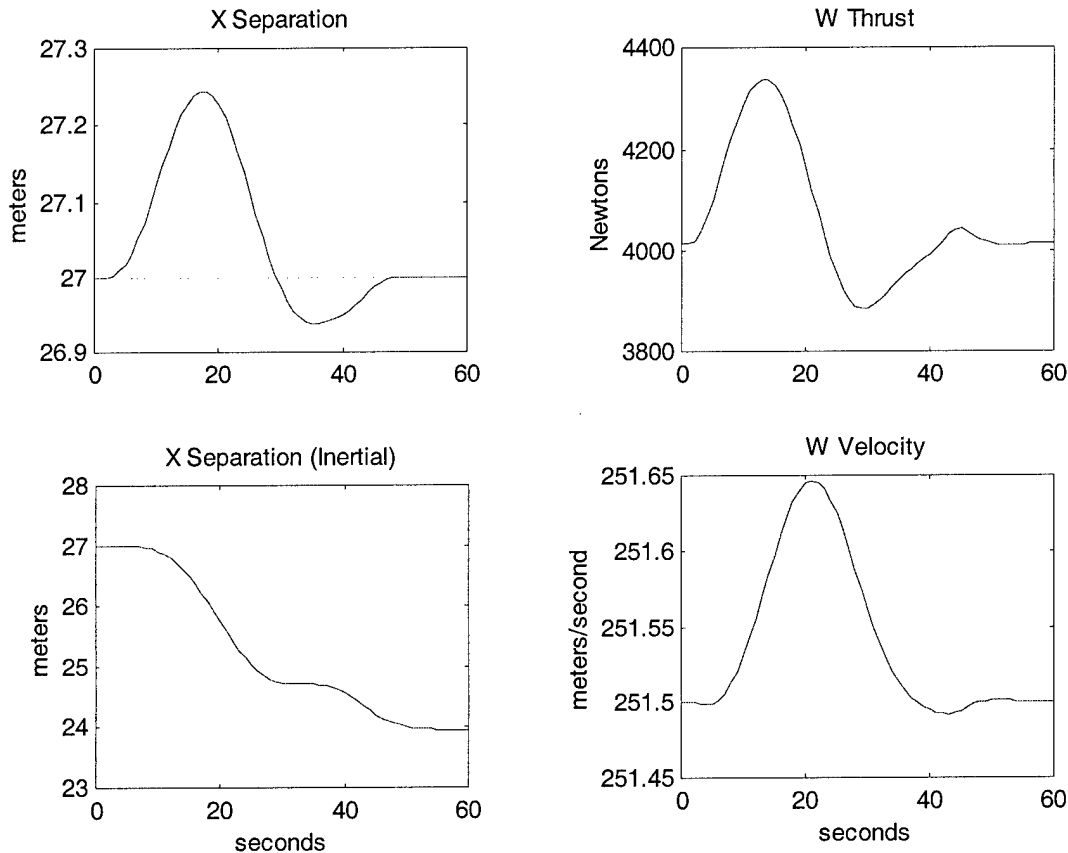


**Figure 20. W's response to positive L heading change: x axis.**

Comparing the x channel response of the primary control system, shown above, with the alternate, shown in Figure 21, the x separation actually decreases during the turn, which is validated by the corresponding increase in velocity. The lift commanded by the

primary controller, see Figure 24, is only slightly less than that commanded by the alternate controller.

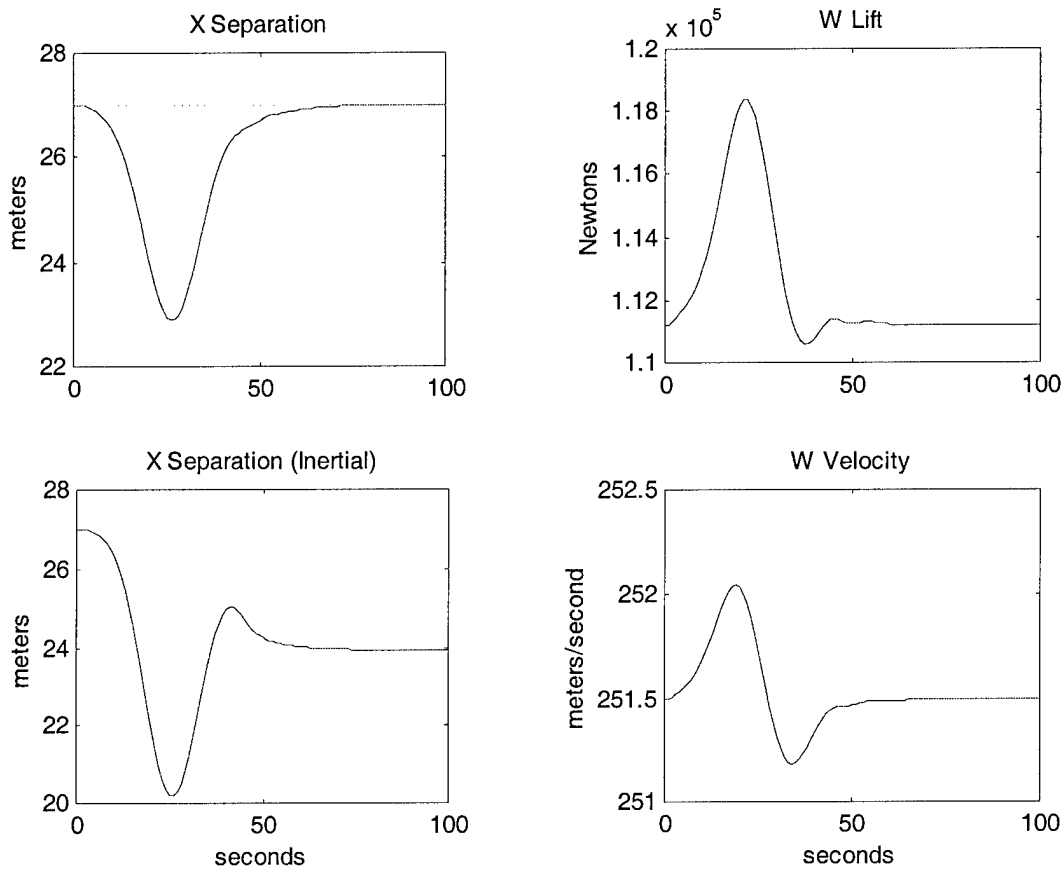


**Figure 21. W's response to positive L heading change: alternate control law: x axis.**

The y separation distances shown in Figure 22 are the results caused by L banking to the left and flying away from W initially and then rolling back to level flight and having W overshoot the commanded y separation distance. Comparing the roll angle of W (Figure 22) with that of L (Figure 19), the time histories are nearly identical, with only a slight overshoot by the control system, as expected. Again the two separation distances

are dramatically different. These distances are the Cartesian components of the total separation distance. The magnitude of the formation separation distance is equal in all reference frames.

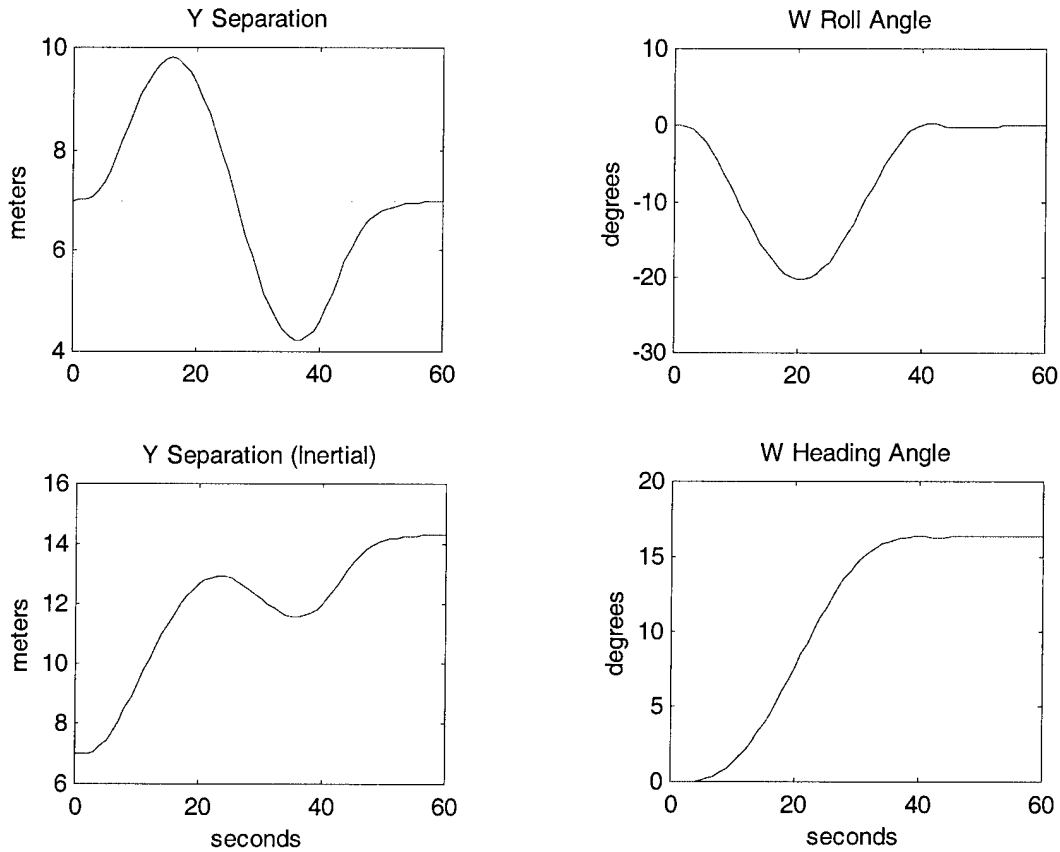


**Figure 22. W's response to positive L heading change: y axis.**

The alternate control law has very little effect on the y channel response, except that the system is slower and the separation distance transients, shown in Figure 23, are greater than for the primary control system. Although the response is different, both

separation distances have the same steady state value as for the primary control system response.

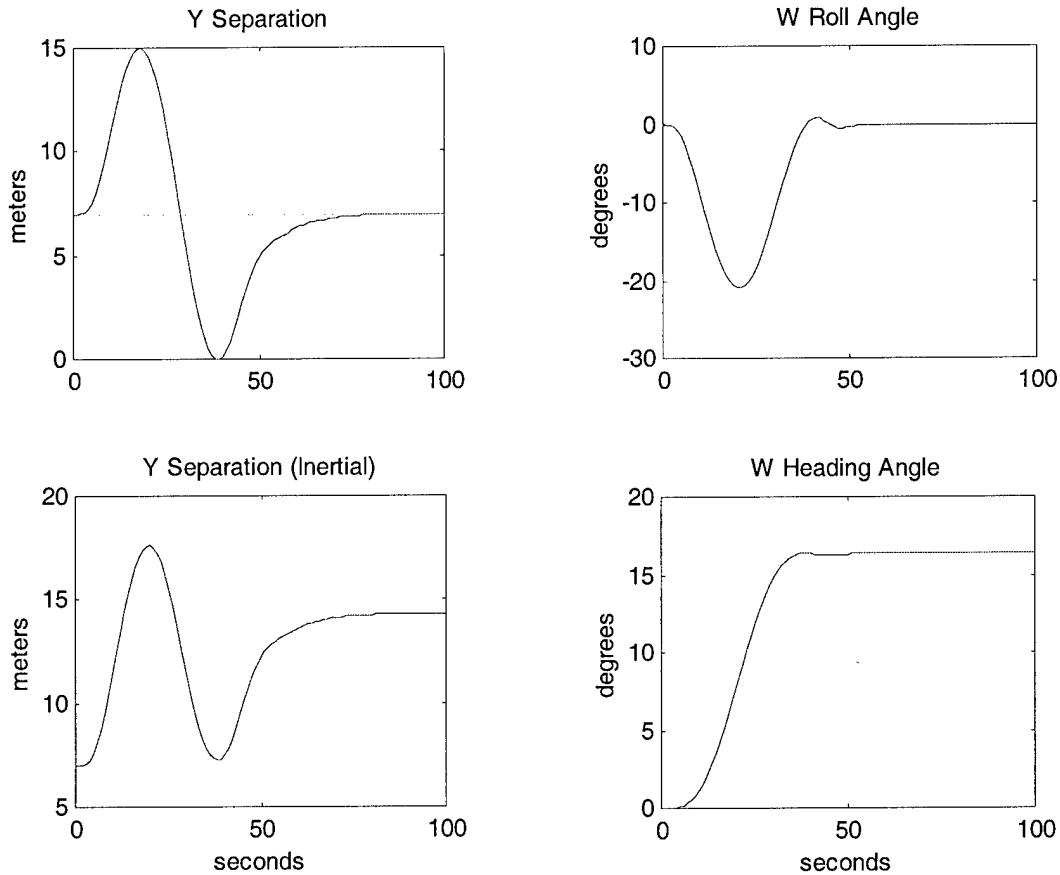


**Figure 23. W's response to positive L heading change: alternate control law: y axis.**

The z channel controller response shown in Figure 24 provided a dramatic increase in lift, as would be expected to maintain altitude during a coordinated turn. Note the large disagreement between the two reference frame measurements of the z separation distance transients. The inertial frame shows a much larger value of z separation, indicating the strong effect of roll angle on measured distances. The comparatively small

value of separation distance in the W frame is the result of the formation turn mode used in the control system, meaning that the controller is trying to keep L in W's x-y plane, as explained in Section 4.2. The separation distance errors used in the controller are measured in W's reference frame.

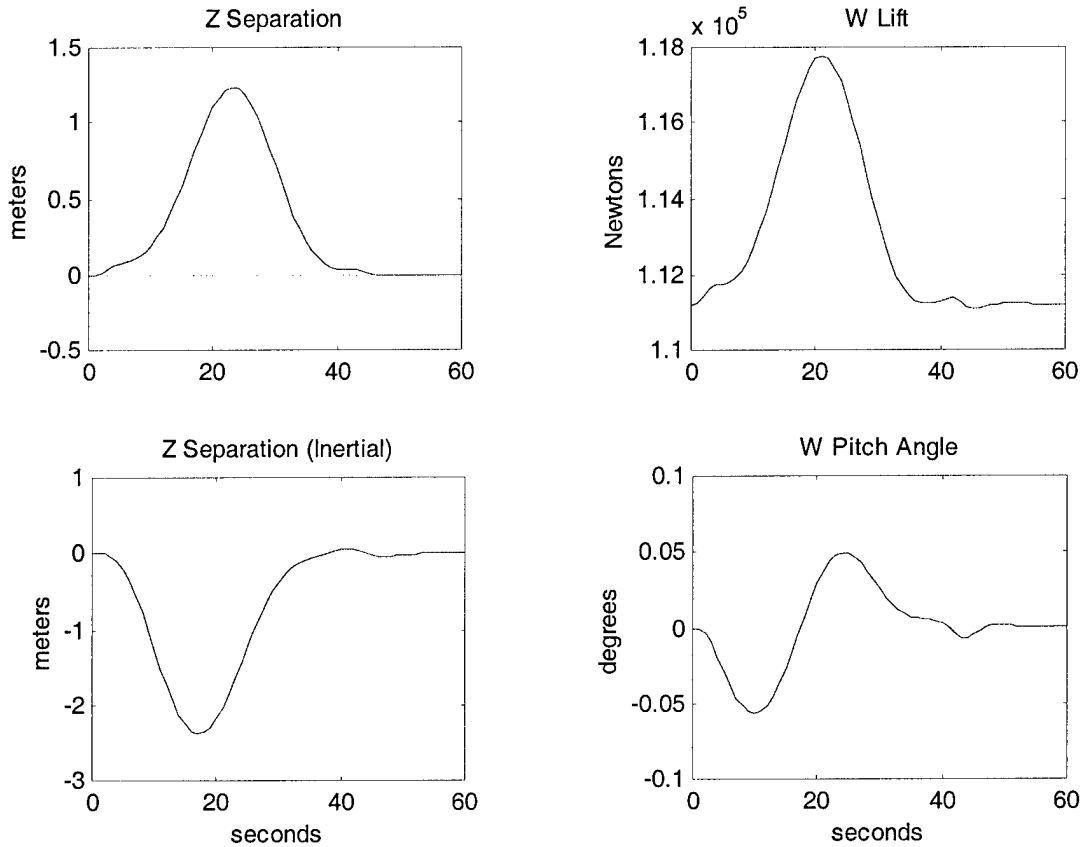


**Figure 24. W's response to positive L heading change: z axis.**

To compare commanded thrust of the two control laws refer to Figure 20 for the primary and Figure 25 for the alternate. The alternate control system requires larger

thrust variations to maintain the formation. As seen in the x and y axes, the separation distance transients are larger for the alternate controller than for the primary.

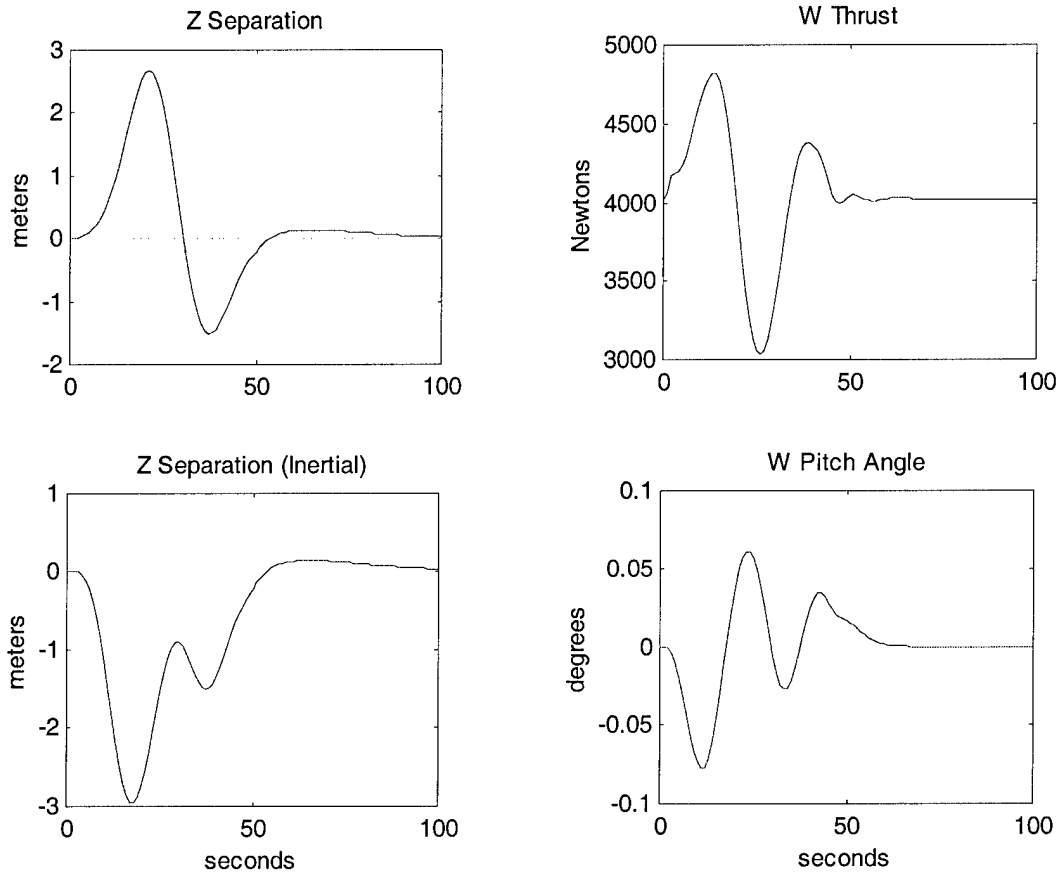


**Figure 25. W's response to positive L heading change: alternate control law: z axis.**

Section 4.2 discusses optional geometry as the formation conducts turning maneuvers. The principal approach in the simulations was to have the controller maintain L in W's x-y plane, which is to say, a z separation distance equal to zero. Figure 26 shows a "route" formation geometry, where the controller maintains L and W flying in

the same inertial x-y plane. Notice that the separation distance in the inertial reference frame is very small compared to the W reference frame.

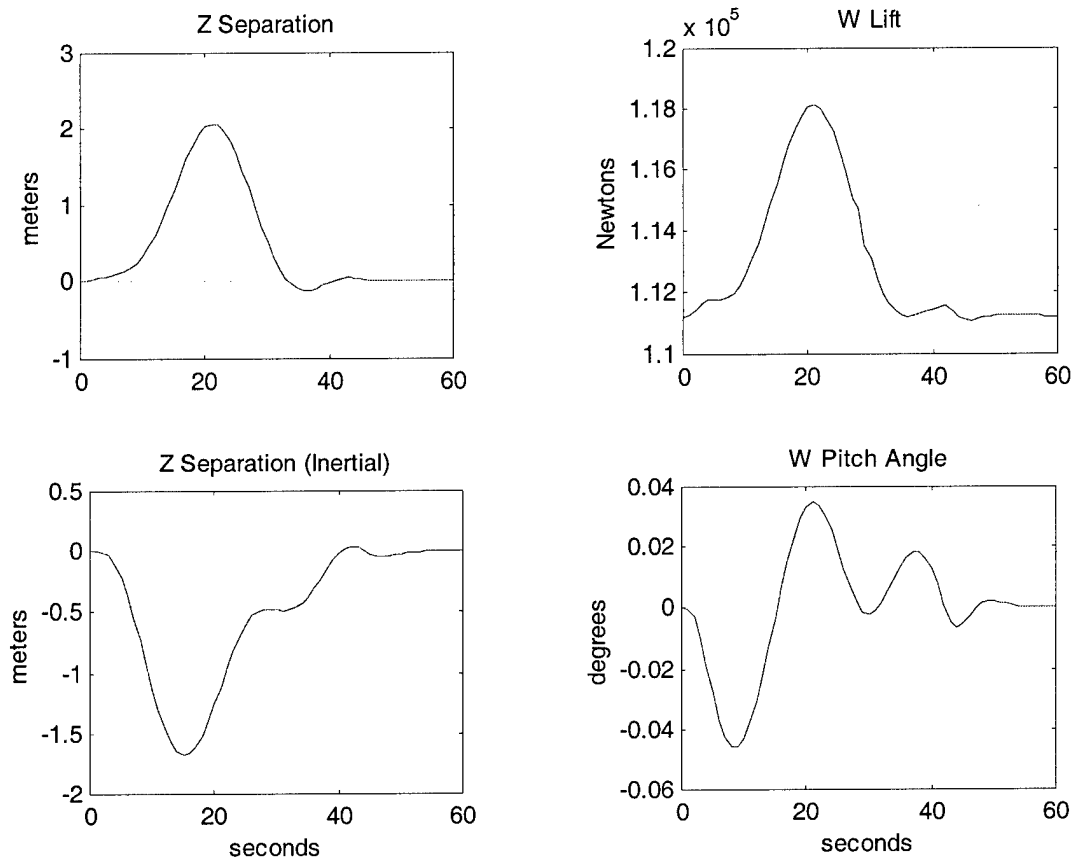


**Figure 26. W's response to positive L heading change: route formation: z axis.**

The next maneuver run in the simulation was a heading change to the right rather than left, or in other words, L is turning to a negative heading angle,  $\psi$ , as shown in the figure below.

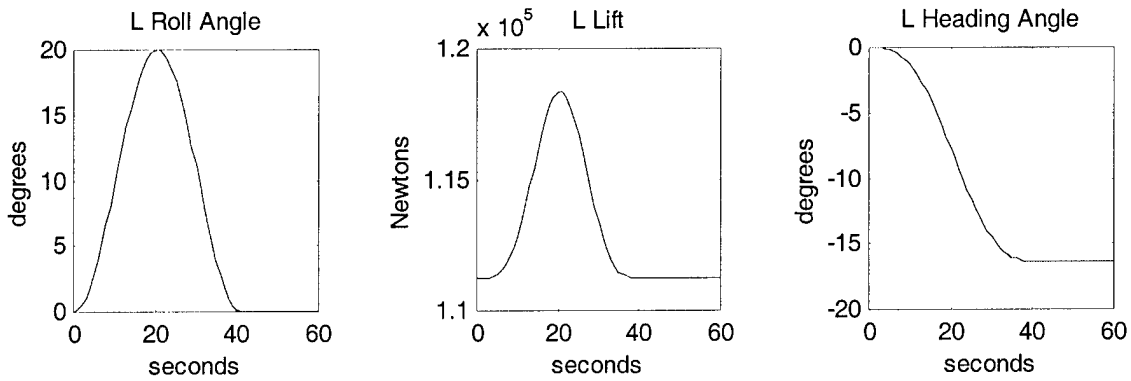


**Figure 27. L negative heading change maneuver.**

When L turns to the right, W is now flying on the short track. Therefore, the controller must reduce W's velocity to prevent overshooting the leader, as shown in Figure 28. As noted previously, the x component of the inertial separation distance reflects the geometry of the formation from a different perspective, but does not change the magnitude of the separation distance.

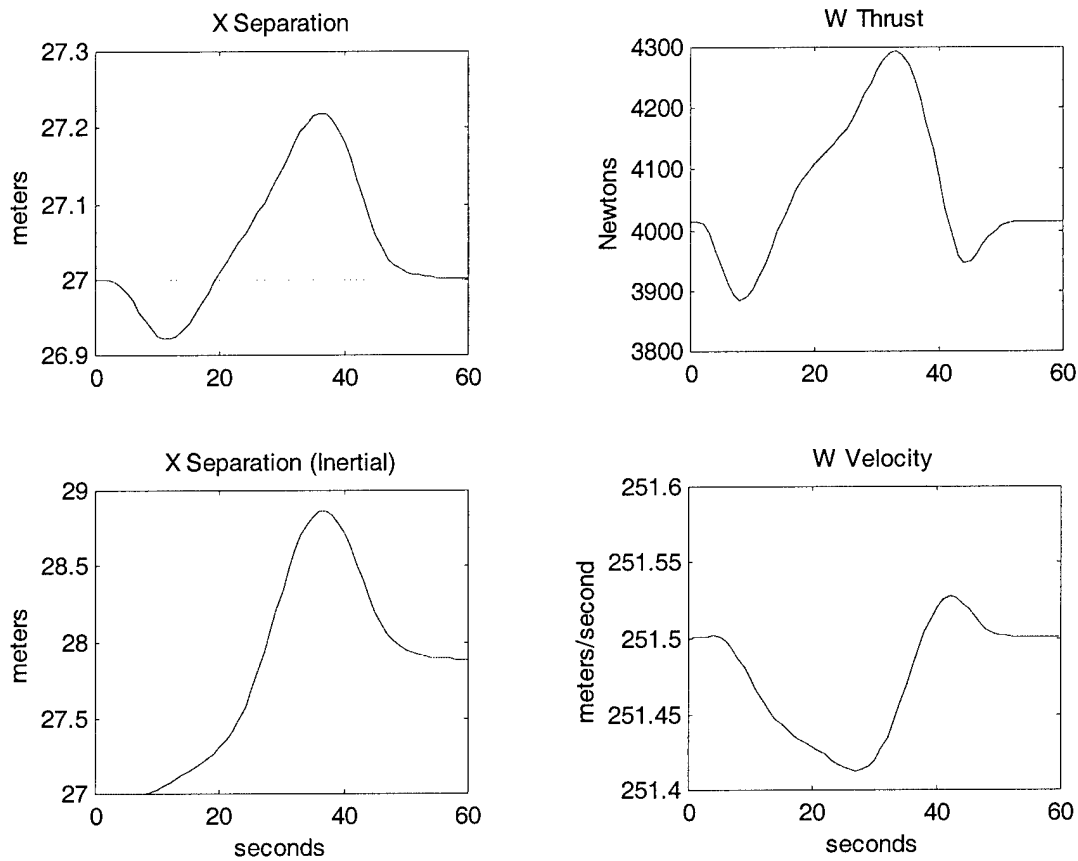


**Figure 28. W's response to negative L heading change: x axis.**

It is evident from Figure 29 that the control system is capable of compensating for the leader turning left or right. Again, the roll angle of W matches L almost perfectly, with only a slight overshoot. The steady state value of inertial separation distance decreased, as expected.

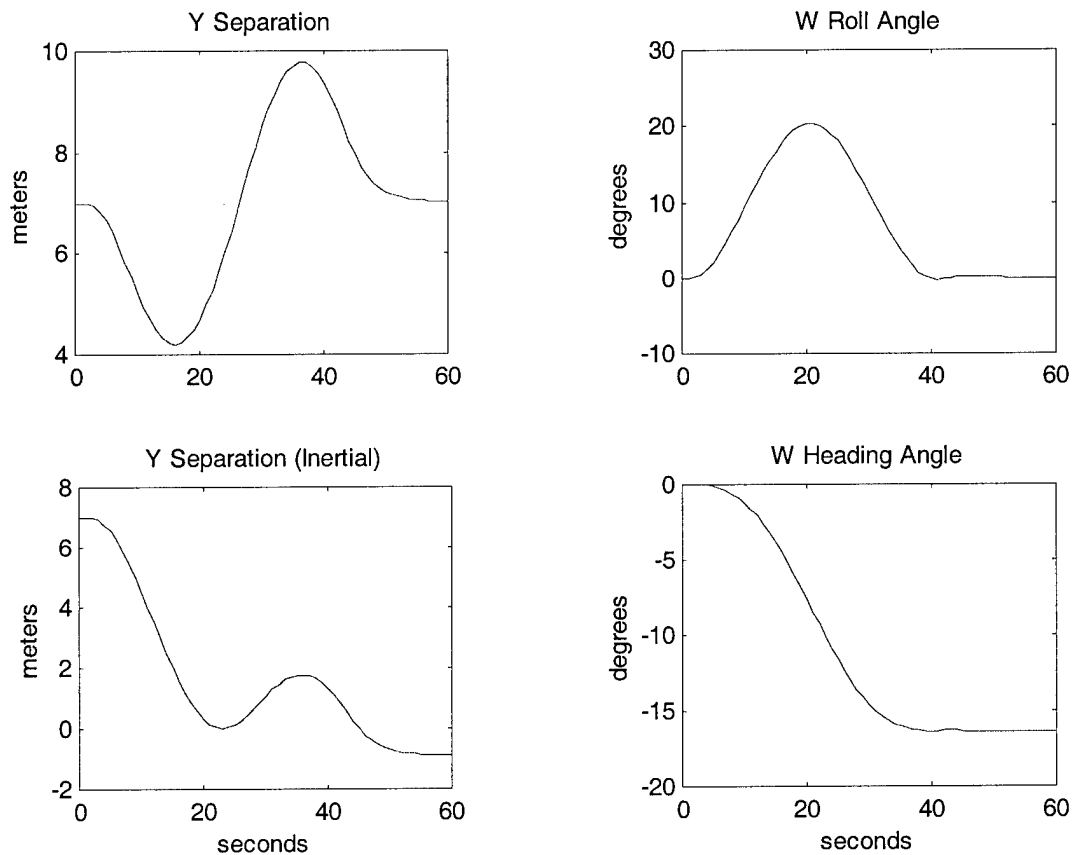


**Figure 29.** W's response to negative L heading change: y axis.

As for the positive heading change, Figure 30 shows a dramatic difference in the z separation of the rotating and inertial reference frame, highlighting the dependency of separation distances on reference frame orientation.

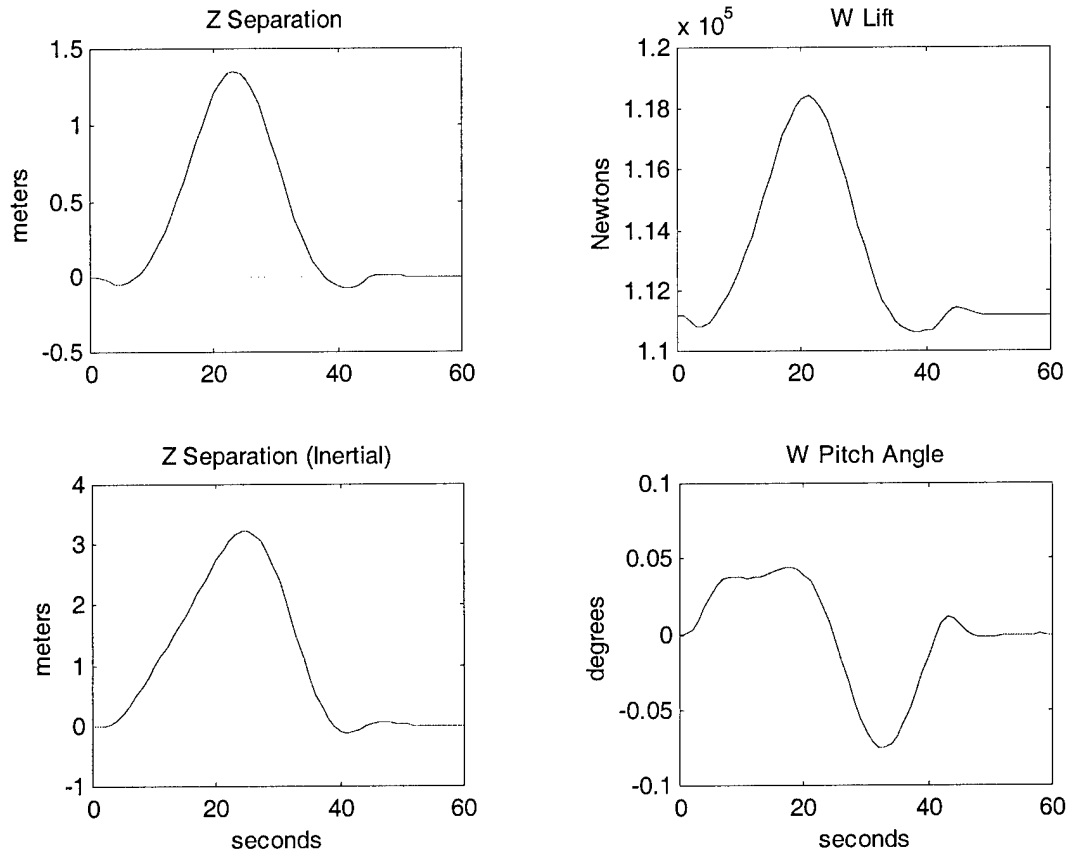
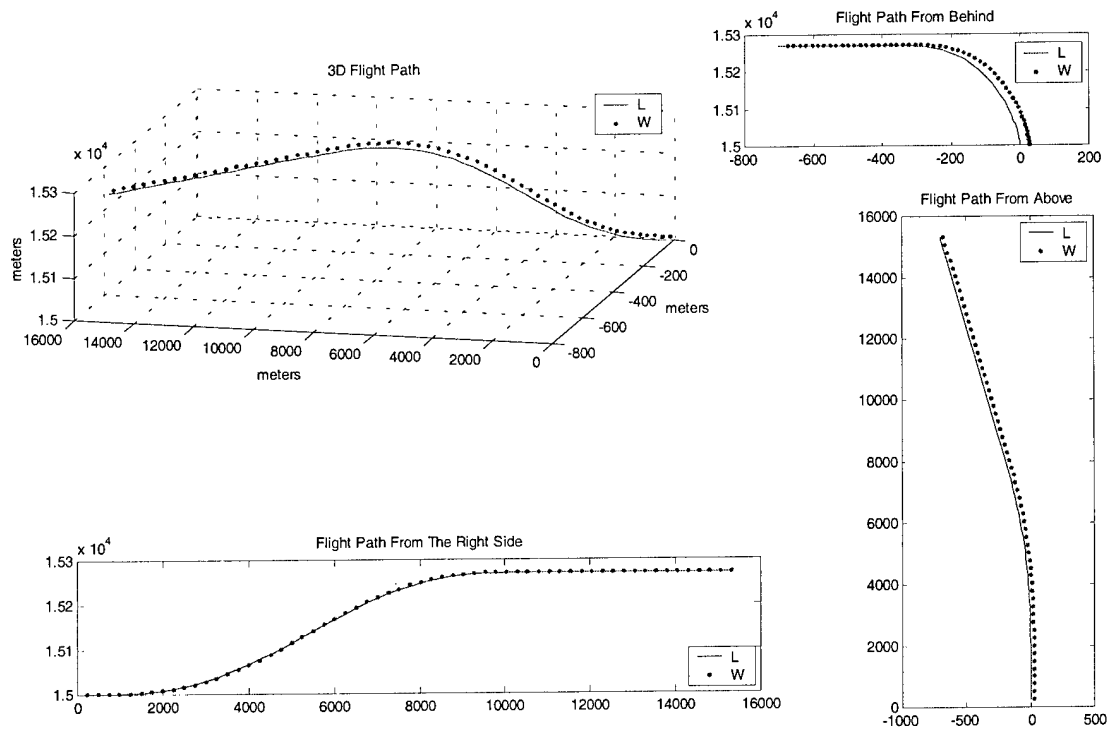


**Figure 30. W's response to negative L heading change: z axis.**

## 5.6 Climbing Turn Maneuver

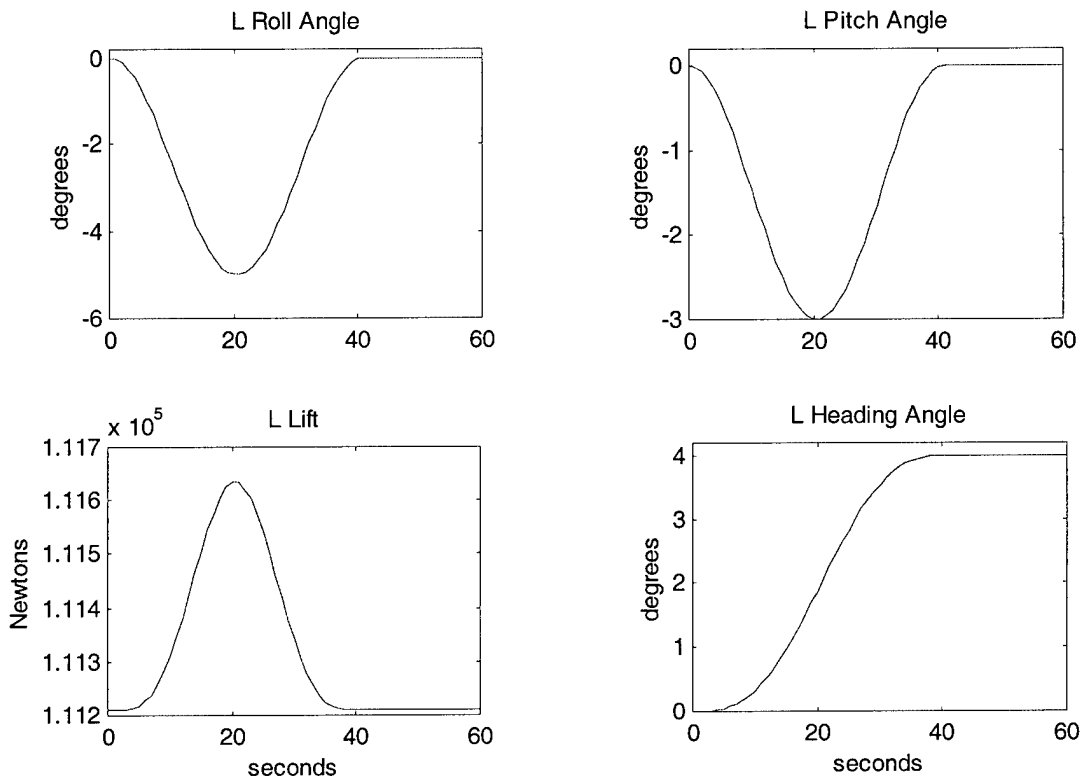
Most complex maneuver conducted in the simulation was the climbing turn.

Figure 31 shows the three dimensional flight path of the formation as it climbed to a new altitude and turned left.



**Figure 31. Flight path in climbing turn maneuver: inertial reference frame.**

To produce the altitude and heading change in the formation, the disturbance signals shown below were created by L. The amount of heading change and the distance climbed for the combined maneuver is less than the individual maneuvers, because the more aggressive maneuvers, when combined together, caused the controller to be unstable.



**Figure 32. L simultaneous altitude and heading change maneuver.**

The next three figures show the formation flight control system performance and the W response, in the three Cartesian axes.

Comparing the thrust required to perform the straight ahead altitude increase (Figure 16) versus the simultaneous altitude and heading change, shown below, it can be

seen that turning while climbing requires significantly more thrust to maintain the formation. Because the heading angle changed less than four degrees, the steady state value of inertial separation distances in both the x and y axis are only slightly different than the W reference frame distances.

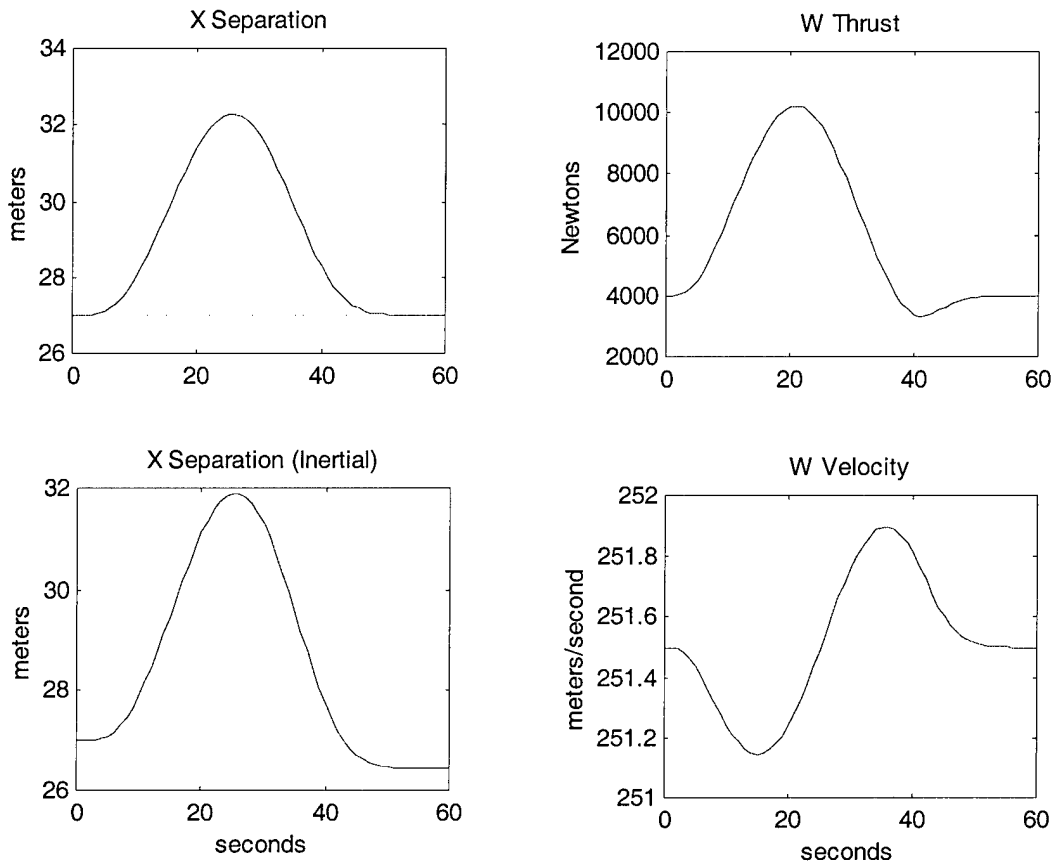


**Figure 33. W's response to the climbing turn maneuver: x axis.**

The y channel of the control system was again able to match the L roll angle to produce the correct heading change with only slight overshoot in spite of the additional complexity of climbing simultaneously, see Figure 34.

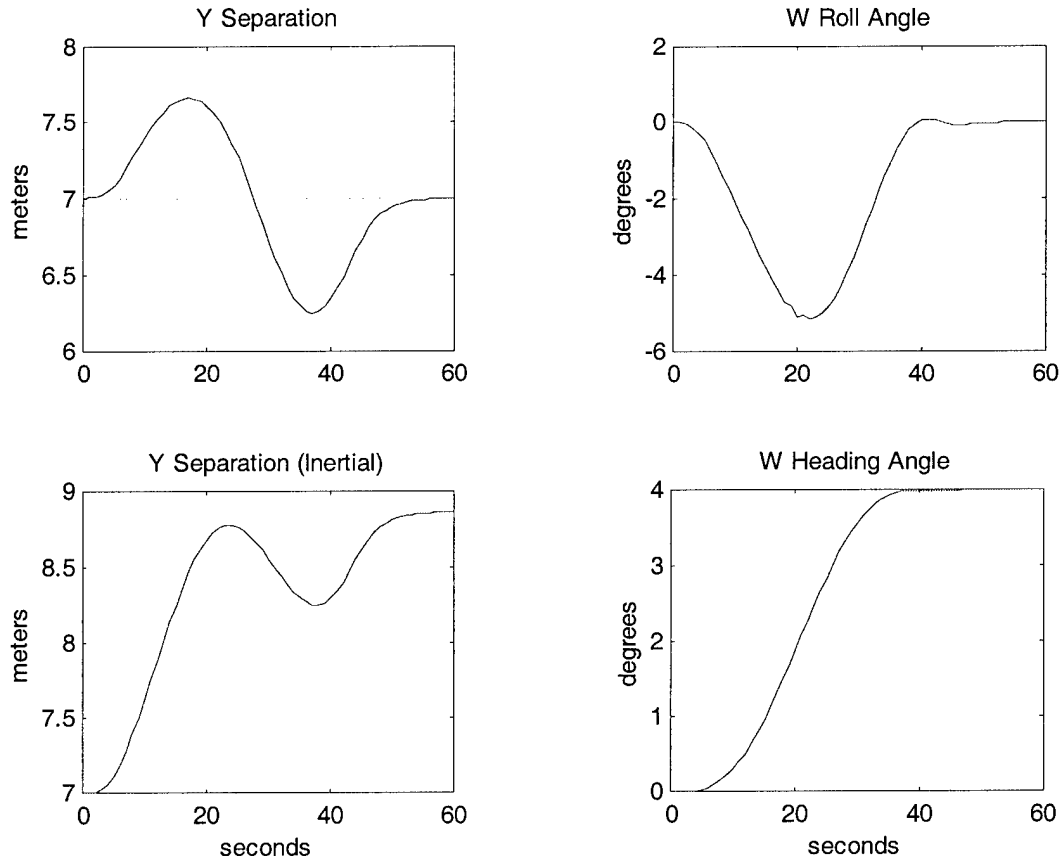


**Figure 34.** W's response to the climbing turn maneuver: y axis.

Inasmuch as the roll angle for the climbing turn had a maximum value of negative five degrees (as opposed to twenty degrees in the constant altitude turns), Figure 35 shows only a small amount of discrepancy between the inertial and rotating reference frame values a z separation distances.

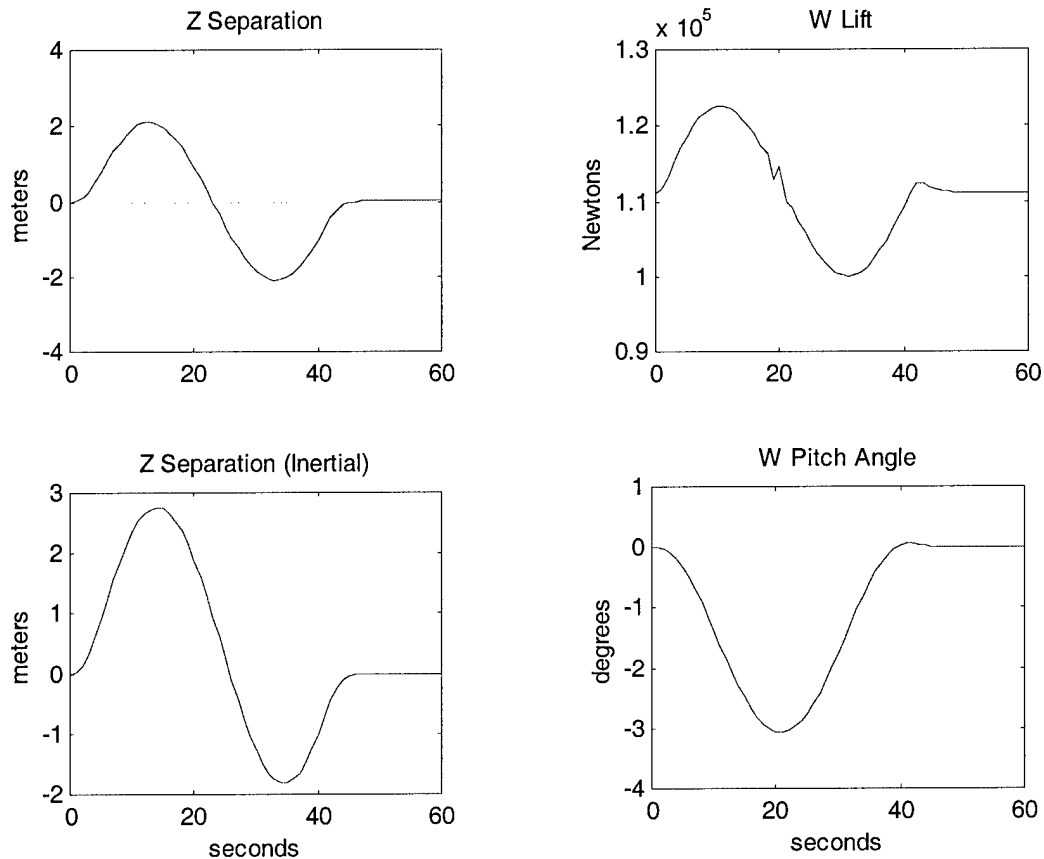


**Figure 35. W's response to the climbing turn maneuver: z axis.**

## 5.7 Formation Flight Control System Gains

Each of the three control variables had proportional control to be responsive to system inputs, integral control to eliminate steady state error, and derivative control to improve system stability. The responsiveness was balanced with the amount of damping for each control variable individually, and each control variable was balanced for the overall system. The final values of the control system gains are listed in Table 2.

**Table 2 Formation Flight Control System Gains**

Title	Symbol	Primary	Alternate	Units
Proportional Control on Thrust	$K_{TP}$	-1000	-130	N/m
Integral Control on Thrust	$K_{TI}$	-1000	-130	N/(m s)
Derivative Control on Thrust	$K_{TD}$	6000	2000	N/(m/s)
Derivative Control on Thrust	$K_{TDD}$	0	5000	N/(m/s <sup>2</sup> )
Proportional Control on Lift	$K_{LP}$	-5000	1300	N/m
Integral Control on Lift	$K_{LI}$	-7000	1000	N/(m s)
Derivative Control on Lift	$K_{LD}$	12000	-10000	N/(m/s)
Derivative Control on Lift	$K_{LDD}$	0	-1000	N/(m/s <sup>2</sup> )
Proportional Control on Roll Rate	$K_{pP}$	0.008	0.0023	rad/(m s)
Proportional Control on Heading Angle	$K_{\psi eP}$	-0.001	0	rad/(m s)
Integral Control on Roll Rate	$K_{pI}$	0.008	0.0023	rad/(m s <sup>2</sup> )
Derivative Control on Roll Rate	$K_{pD}$	-0.050	-0.025	rad/m
Derivative Control on Roll Rate	$K_{pDD}$	-0.050	-0.025	rad/(m/s)

The magnitude of the gains can be misleading until one recognizes the units associated each control element.

## **6 Conclusions and Recommendations**

### **6.1 Conclusions**

The results of the nonlinear simulations validate the concept of three dimensional automatic formation flight control. However, both the primary and the alternate control systems are very sensitive to the amplitude of disturbances, which is to say that aggressive L maneuvers can cause the controllers to be unstable. Control system robustness will become even more crucial when the aerodynamic effects of close formation flight are included in the simulation. Indeed the induced drag reduction afforded by close formation flight requires W to stay within  $\pm 5\%$  of the optimal lateral separation during formation maneuvers, further limiting the amplitude of permissible L maneuvers. Hence, the maneuvers performed by L must be relatively benign for the controller to automatically maintain the formation and the benefit.

### **6.2 Recommendations**

Further research on this project could be accomplished in several different areas:

1. The simulation equations of motion could be linearized.
2. The aerodynamic coupling effects of close formation flight should be modeled in three dimensions and included in the simulation.
3. Moment relationships should be derived and included in the simulation.

4. The current control law could be modified to allow thrust to be affected by  $z$  separation error and lift to be affected by  $x$  separation control error to reflect the manner in which pilots control their aircraft.
5. The type of formation flown during turns can be changed to either of the other two types described in Section 4.1.

## Appendix A

The formation flight simulations were accomplished using two Matlab script files, one to drive the simulations and one that contained the differential equations of motion. The Matlab solver routine used to do the numerical integration was called ODE23.

### Simulation Driver Program

```
%cffc_sim_a.m
global mw ml g rho Cdw Kw Sw Ll phil Yw Vl gammal;
global xc yc zc KTI KLI KpI;
    %Flight altitude of 15,000 m
h=15000; rho=0.19475; g=9.81;
    %L aircraft parameters
Sl=27.87; Llbar=111210; Cdol=.015; Kl=.02; ml=Llbar/g; %11336.4;
    %L drag relationships
Vlbar=251.5;
qlbar=.5*rho*Vlbar^2;
Dlbar=(Cdol+Kl*(Llbar/(qlbar*Sl))^2)*qlbar*Sl;
Tlbar=Dlbar;
    %L trim values
Vl=251.5; gammal=0; Tl=Tlbar; Ll=Llbar; phil=0; psil=0;
    %W aircraft parameters
Sw=27.87; Lwbar=111210; Cdw=.015; Kw=.02; mw=Lwbar/g; %11336.4;
    %W drag relationships
Vwbar=251.5; qwbar=.5*rho*Vwbar^2;
Dwbar=(Cdw+Kw*(Lwbar/(qwbar*Sw))^2)*qwbar*Sw;
Twbar=Dwbar;
    %W trim values
uw=0; gammaw=0; phiw=0; psiw=0; Yw=0;
    %Commanded separation in the W reference frame
xc=27; yc=7; zc=0;
    %X channel controller gains
KTI=-1000;
KTP=-1000;
KTD=6000;
    %Z channel controller gains
KLI=-7000;
KLP=-5000;
KLD=12000;
    %Y channel controller gains
KpI=.0080;
KpP=.0080;
KpsiP=-.0010;
KpD=-.050;
KpDD=-.050;
    %Alternate control law Z channel controller gains
```

```

%KTI=-130;
%KTP=-130;
%KTD=2000;
%KTDD=5000;
    % Alternate control law X channel controller gains
%KLI=1000;
%KLP=1300;
%KLD=-10000;
%KLDD=-1000;
    % Alternate control law Y channel controller gains
%KpI=.0023;
%KpP=.0023;
%KpsiP=0;
%KpD=-.025;
%KpDD=-.025;
    %Initialize the program variables
t=60;
dt=.1;
n=t/dt+1; nn=410; nnn=0; j=0;
xv=0; zv=0; yv=0; ya=0;
CWI=[1 0 0;0 1 0;0 0 1];
CLI=[1 0 0;0 1 0;0 0 1];
YI=[]; YY=[]; L=[]; LP=[]; LR=[]; WI=[];
pathl=[]; pathL=[]; pathw=[]; pathW=[]; dh=[];
    %Initial conditions for the numerical integration routine
Y0=[Vwbar gammaw phiw psiw 27 7 0 Twbar Lwbar uw psil];
for i=1:n;
    %Build the solution matrices
YI=[YI;Y0];
if rem(nnn,1/dt)==0;
    YY=[YY;Y0];
end
    %Call the differential equation solver
[t,Y]=ode23('cffc_sim_al',[0 dt],Y0');
DL=length(t);
    %L flight disturbances for pitch and roll
if i<=nn;
Vl=Vlbar-5*(1+cos(pi+((i-1)*pi/(nn-1))));
gammal=(-3/(2*57.3))*(1+cos(pi+(2*(i-1)*pi/(nn-1))));h=h-
Vl*sin(gammal)*dt;
phil=(-5/(2*57.3))*(1+cos(pi+(2*(i-1)*pi/(nn-1)))); Ll=Llbar/cos(phil);
end
    %Create derivatives of relative position variables
if i>=4;
xv=(YI(i,5)-YI(i-1,5))/dt;
zv=(YI(i,7)-YI(i-1,7))/dt;
yv=(YI(i,6)-YI(i-1,6))/dt;
ya=((YI(i,6)-YI(i-1,6))-(YI(i-2,6)-YI(i-3,6)))/dt^2);
end
    %Update initial conditions for next integration time step
Y0=Y(DL,:);
Y0(8)=(Twbar/cos(Y(DL,2)))+KTP*(xc-Y(DL,5))+KTD*xv;
Y0(9)=(Lwbar/cos(Y(DL,2)))+KLP*(zc-Y(DL,7))+KLD*zv;
Y0(10)=KpP*(yc-Y(DL,6))+KpsiP*(Y(DL,11)-Y(DL,4))+KpD*yv+KpDD*ya;
    %Alternate control law derivatives of relative position variables

```

```

%if i>=4;
%xv=(YI(i,5)-YI(i-1,5))/dt;
%xa=((YI(i,5)-YI(i-1,5))-(YI(i-2,5)-YI(i-3,5)))/dt^2;
%zv=(YI(i,7)-YI(i-1,7))/dt;
%za=((YI(i,7)-YI(i-1,7))-(YI(i-2,7)-YI(i-3,7)))/dt^2;
%yv=(YI(i,6)-YI(i-1,6))/dt;
%ya=((YI(i,6)-YI(i-1,6))-(YI(i-2,6)-YI(i-3,6)))/dt^2;
%end

%Alternate control law initial conditions for integration
%Y0=Y(DL,:);
%Y0(8)=(Twbar/cos(Y(DL,2)))+KTP*(zc-Y(DL,7))+KTD*zv+KTDD*za;
%Y0(9)=(Lwbar/cos(Y(DL,2)))+KLP*(xc-Y(DL,5))+KLD*xv+KLDD*xa;
%Y0(10)=KpP*(yc-Y(DL,6))+KpsiP*(Y(DL,11)-Y(DL,4))+KpD*yv+KpDD*ya

%Transform error signals
%e=CWI*[xc-Y(DL,5);yc-Y(DL,6);zc-Y(DL,7)];
%e=-CLI'*CWI*[xc-Y(DL,5);yc-Y(DL,6);zc-Y(DL,7)];
%Y0=Y(DL,:);
%Y0(8)=(Twbar/cos(Y(DL,2)))+KTP*(e(1))+KTD*xv;
%Y0(9)=(Lwbar/cos(Y(DL,2)))+KLP*(e(3))+KLD*zv;
%Y0(10)=KpP*(e(2))+KpsiP*(Y(DL,11)-Y(DL,4))+KpD*yv+KpDD*ya;

%Rotating reference frame transformation
CWI11=cos(Y0(4)-Y0(11))*cos(Y0(2));
CWI12=sin(Y0(4)-Y0(11))*cos(Y0(3))+cos(Y0(4)-
Y0(11))*sin(Y0(2))*sin(Y0(3));
CWI13=sin(Y0(4)-Y0(11))*sin(Y0(3))+cos(Y0(4)-
Y0(11))*sin(Y0(2))*cos(Y0(3));
CWI21=-sin(Y0(4)-Y0(11))*cos(Y0(2));
CWI22=cos(Y0(4)-Y0(11))*cos(Y0(3))-sin(Y0(4)-
Y0(11))*sin(Y0(2))*sin(Y0(3));
CWI23=-cos(Y0(4)-Y0(11))*sin(Y0(3))-sin(Y0(4)-
Y0(11))*sin(Y0(2))*cos(Y0(3));
CWI31=sin(Y0(2));
CWI32=-cos(Y0(2))*sin(Y0(3));
CWI33=cos(Y0(2))*cos(Y0(3));
CWI=[CWI11 CWI12 CWI13;CWI21 CWI22 CWI23;CWI31 CWI32 CWI33];

%Rotating reference frame transformation (L to I)
%CLI11=cos(Y0(11))*cos(gammal);
%CLI12=cos(Y0(11))*sin(gammal)*sin(phil)-sin(Y0(11))*cos(phil);
%CLI13=sin(Y0(11))*sin(phil)+cos(Y0(11))*sin(gammal)*cos(phil);
%CLI21=sin(Y0(11))*cos(gammal);
%CLI22=cos(Y0(11))*cos(phil)+sin(Y0(11))*sin(gammal)*sin(phil);
%CLI23=-cos(Y0(11))*sin(phil)+sin(Y0(11))*sin(gammal)*cos(phil);
%CLI31=-sin(gammal);
%CLI32=cos(gammal)*sin(phil);
%CLI33=cos(gammal)*cos(phil);
%CLI=[CLI11 CLI12 CLI13;CLI21 CLI22 CLI23;CLI31 CLI32 CLI33];

%Inertial separation and ground track calculations
if rem(nnn,1/dt)==0;
j=j+1;
WI=[WI;[CWI*[Y(DL,5);Y(DL,6);Y(DL,7)]]'];
pathl=[pathl;[-Vl*sin(Y(DL,11)) Vl*cos(Y(DL,11)) Ll]];
pathL=[pathL;[sum(pathl(:,1)) sum(pathl(:,2)) h]];
pathw=[pathw;[-Y(DL,1)*sin(Y(DL,4)) Y(DL,1)*cos(Y(DL,4))]];
pathW=[pathW;[sum(pathw(:,1))+WI(j,1) sum(pathw(:,2))-WI(j,2) h-
WI(j,3)]];

```

```

        %L flight path in pitch and roll
L=[L;Vl];
LP=[LP;gamma*57.3];
LR=[LR;phi*57.3];
end
nnn=nnn+1;
end
ts=[0:1:(n-1)*dt];
    %xyz displacement output
tts=[0:1:(n-1)*dt];
figure(1),subplot(3,2,1),plot(tts,YI(:,5),tts,xc);title('X
Separation');
subplot(3,2,2),plot(tts,YI(:,8));title('W Thrust');
subplot(3,2,3),plot(tts,YI(:,6),tts,yc);title('Y Separation');
subplot(3,2,4),plot(tts,YI(:,3)*57.3);title('W Bank Angle');
subplot(3,2,5),plot(tts,YI(:,7),tts,zc);title('Z Separation')
subplot(3,2,6),plot(tts,YI(:,9));title('W Lift');
    %Velocity change output
figure(2),subplot(2,2,1),plot(ts,L(:,1));title('L Velocity');
subplot(2,2,2),plot(ts,YY(:,1));title('W Velocity');
subplot(2,2,3),plot(ts,YY(:,5),ts,xc);title('X Separation');
subplot(2,2,4),plot(ts,YY(:,8));title('W Thrust');
    %Altitude change output
figure(3),subplot(3,2,1),plot(ts,YY(:,5),ts,xc);title('X Separation');
subplot(3,2,2),plot(ts,YY(:,8));title('W Thrust');
subplot(3,2,3),plot(ts,YY(:,7),ts,zc);title('Z Separation')
subplot(3,2,4),plot(ts,YY(:,9));title('W Lift');
subplot(3,2,5),plot(ts,YY(:,2)*57.3);title('W Pitch Angle');
subplot(3,2,6),plot(ts,pathL(:,3));title('Formation Altitude Change');
    %Heading change output
figure(4),subplot(2,2,1),plot(ts,YY(:,5),ts,xc);title('X Separation');
subplot(2,2,2),plot(ts,YY(:,8));title('W Thrust');
subplot(2,2,3),plot(ts,WI(:,1));title('X Separation (Inertial)');
subplot(2,2,4),plot(ts,YY(:,1));title('W Velocity');
figure(5),subplot(2,2,1),plot(ts,YY(:,6),ts,yc);title('Y Separation');
subplot(2,2,2),plot(ts,YY(:,3)*57.3);title('W Roll Angle');
subplot(2,2,3),plot(ts,WI(:,2));title('Y Separation (Inertial)');
subplot(2,2,4),plot(ts,YY(:,4)*57.3);title('W Heading Angle');
figure(6),subplot(2,2,1),plot(ts,YY(:,7),ts,zc);title('Z Separation');
subplot(2,2,2),plot(ts,YY(:,9));title('W Lift');
subplot(2,2,3),plot(ts,WI(:,3));title('Z Separation (Inertial)');
subplot(2,2,4),plot(ts,YY(:,2)*57.3);title('W Pitch Angle');
figure(7),subplot(2,2,1),plot(ts,LR(:,1));title('L Roll Angle');
subplot(2,2,2),plot(ts,LP(:,1));title('L Pitch Angle');
subplot(2,2,3),plot(ts,pathL(:,3));title('L Lift');
subplot(2,2,4),plot(ts,YY(:,11)*57.3);title('L Heading Angle');
    %Three dimensional turn output
figure(8),subplot(2,2,1),plot3(pathL(:,1),pathL(:,2),pathL(:,3),pathW(
:,1),pathW(:,2),pathW(:,3),'.');
title('3D Flight Path');legend('L','W');grid on
subplot(2,2,2),plot(pathL(:,1),pathL(:,3),pathW(:,1),pathW(:,3),'.');
title('Flight Path From Behind');legend('L','W');
subplot(2,2,3),plot(pathL(:,2),pathL(:,3),pathW(:,2),pathW(:,3),'.');
title('Flight Path From The Right Side');legend('L','W');
subplot(2,2,4),plot(pathL(:,1),pathL(:,2),pathW(:,1),pathW(:,2),'.');

```

```

title('Flight Path From Above');legend('L','W');
    %Alternate control law xyz displacement output
    %tts=[0:1:(n-1)*dt];
    %figure(1),subplot(3,2,1),plot(tts,YI(:,5),tts,xc);title('X Separation');
    %subplot(3,2,2),plot(tts,YI(:,9));title('W Lift');
    %subplot(3,2,3),plot(tts,YI(:,6),tts,yc);title('Y Separation');
    %subplot(3,2,4),plot(tts,YI(:,3)*57.3);title('W Bank Angle');
    %subplot(3,2,5),plot(tts,YI(:,7),tts,zc);title('Z Separation')
    %subplot(3,2,6),plot(tts,YI(:,8));title('W Thrust');
    %Alternate control law Velocity change output
    %figure(2),subplot(3,2,1),plot(ts,L(:,1));title('L Velocity');
    %subplot(3,2,3),plot(ts,YY(:,1));title('W Velocity');
    %subplot(3,2,4),plot(ts,YY(:,5),ts,xc);title('X Separation');
    %subplot(3,2,5),plot(ts,YY(:,9));title('W Lift');
    %subplot(3,2,6),plot(ts,YY(:,8));title('W Thrust');
    % Alternate control law Altitude change output
    %figure(3),subplot(3,2,1),plot(ts,YY(:,5),ts,xc);title('X Separation');
    %subplot(3,2,2),plot(ts,YY(:,9));title('W Lift');
    %subplot(3,2,3),plot(ts,YY(:,7),ts,zc);title('Z Separation')
    %subplot(3,2,4),plot(ts,YY(:,8));title('W Thrust');
    %subplot(3,2,5),plot(ts,YY(:,2)*57.3);title('W Pitch Angle');
    %subplot(3,2,6),plot(ts,pathL(:,3),ts,pathW(:,3),'.');title('Altitude
Change');
    % Alternate control law Heading change output
    %figure(4),subplot(2,2,1),plot(ts,YY(:,5),ts,xc);title('X Separation');
    %subplot(2,2,2),plot(ts,YY(:,9));title('W Lift');
    %subplot(2,2,3),plot(ts,WI(:,1));title('X Separation (Inertial)');
    %subplot(2,2,4),plot(ts,YY(:,1));title('W Velocity');
    %figure(5),subplot(2,2,1),plot(ts,YY(:,6),ts,yc);title('Y Separation');
    %subplot(2,2,2),plot(ts,YY(:,2)*57.3);title('W Roll Angle');
    %subplot(2,2,3),plot(ts,WI(:,2));title('Y Separation (Inertial)');
    %subplot(2,2,4),plot(ts,YY(:,4)*57.3);title('W Heading Angle');
    %figure(6),subplot(2,2,1),plot(ts,YY(:,7),ts,zc);title('Z Separation');
    %subplot(2,2,2),plot(ts,YY(:,8));title('W Thrust');
    %subplot(2,2,3),plot(ts,WI(:,3));title('Z Separation (Inertial)');
    %subplot(2,2,4),plot(ts,YY(:,2)*57.3);title('W Pitch Angle');
    %figure(7),subplot(2,2,1),plot(ts,LR(:,1));title('L Roll Angle');
    %subplot(2,2,2),plot(ts,LP(:,1));title('L Pitch Angle');
    %subplot(2,2,3),plot(ts,pathL(:,3));title('L Lift');
    %subplot(2,2,4),plot(ts,YY(:,11)*57.3);title('L Heading Angle');

```

#### Simulation Equations of Motion

```

    %Differenctial Equations of formation model
function eqn=cffc_sim_al(t,Y);
global mw ml g rho Cdw Kw Sw Ll phil Yw Vl gammal;
global xc yc zc KTI KLI KpI;
    % Vw=Y(1); gammaw=Y(2); phiw=Y(3); psiw=Y(4); x=Y(5); y=Y(6);
z=Y(7);
    % Tw=Y(8); Lw=Y(9); p=Y(10);
    %psil=Y(11);
    %Initialize solution vector
eqns=[];
    %Solve for dynamic pressure
qw=.5*rho*Y(1)^2;

```

```

%Rotating reference frame transformation
c1=cos(Y(2))*cos(gammal)*cos(Y(11)-Y(4))+sin(Y(2))*sin(gammal);
c2=sin(Y(2))*cos(gammal)*sin(Y(3))*cos(Y(11)-
Y(4))+cos(gammal)*cos(Y(3))*sin(Y(11)-Y(4))-
cos(Y(2))*sin(gammal)*sin(Y(3));
c3=sin(Y(2))*cos(gammal)*cos(Y(3))*cos(Y(11)-Y(4))-
cos(gammal)*sin(Y(3))*sin(Y(11)-Y(4))-cos(Y(2))*sin(gammal)*cos(Y(3));
%Differential equations of motion
DY1=((Y(8)-(Cdw*qw*Sw+Kw*((Y(9))^2)/(qw*Sw)))/mw)+g*sin(Y(2));
DY2=(-Y(9)*cos(Y(3))/(mw*Y(1)))+(g*cos(Y(2)))/Y(1)-
(Yw*sin(Y(3))/(mw*Y(1)));
DY3=Y(10);
DY4=((-Y(9)*sin(Y(3))+Yw*cos(Y(3)))/(mw*Y(1)*cos(Y(2))));
DY5=((-Y(6)*g*cos(Y(2))*sin(Y(3))-
Y(7)*g*cos(Y(2))*cos(Y(3)))/Y(1))+((Y(6)*Yw+Y(7)*Y(9))/(mw*Y(1)))-
Y(1)+Vl*c1;
DY6=Y(7)*Y(10)+((Y(7)*tan(Y(2))*(Y(9)*sin(Y(3))-Yw*cos(Y(3)))-
Y(5)*Yw)/(mw*Y(1)))+(Y(5)*g*cos(Y(2))*sin(Y(3)))/Y(1)+Vl*c2;
DY7=-Y(6)*Y(10)+((-Y(6)*tan(Y(2))*(Y(9)*sin(Y(3))-Yw*cos(Y(3)))-
Y(5)*Y(9))/(mw*Y(1)))+(Y(5)*g*cos(Y(2))*cos(Y(3)))/Y(1)+Vl*c3;
%Controller equations
DY8=KTI*(xc-Y(5));
DY9=KLI*(zc-Y(7));
DY10=KpI*(yc-Y(6));
%Alternate control law controller equations
%DY8=KTI*(zc-Y(7));
%DY9=KLI*(xc-Y(5));
%DY10=KpI*(yc-Y(6));
%Transform error signals
%e=CWI*[xc-Y(5);yc-Y(6);zc-Y(7)];
%e=-CLI'*CWI*[xc-Y(5);yc-Y(6);zc-Y(7)];
%Controller equations for different turn formations
%DY8=KTI*(e(1));
%DY9=KLI*(e(3));
%DY10=KpI*(e(2));
%L heading equation
DY11=(-Ll*sin(phil)/(ml*Vl*cos(gammal)));
%Solution Vector
eqn=[eqns DY1 DY2 DY3 DY4 DY5 DY6 DY7 DY8 DY9 DY10 DY11]';

```

## Bibliography

- [1] Meyers, K. Jacobsen, Convair B-36. A Complete History of America's 'Big Stick', Schiffer Publishing Ltd, 1997.
- [2] Anderson, C. E., "Aircraft Wingtip Coupling Experiments," *Aerophile* Vol 2 No 4, Dec 1980.
- [3] Kuethe, Arnold M. and Chuen-Yen Chow, Foundations of Aerodynamics: Bases of Aerodynamic Design, Third Edition. John Wiley & Sons, 1976.
- [4] Crow, S.C., "Stability Theory for a Pair of Trailing Vortices." *American Institute of Aeronautics and Astronautics Journal*, Vol. 8, No. 12, December 1970.
- [5] Kopp, Friedrich; "Doppler Lidar Investigation of Wake Vortex Transport Between Closely Spaced Parallel Runways." *American Institute of Aeronautics and Astronautics Journal*, Vol. 32, No. 4, April 1994.
- [6] Beukenberg, Markus, Dietrich Hummel, "Aerodynamics, Performance and Control of Airplanes in Formation Flight." ICAS-90-5.9.3.
- [7] Maskew, Brian; "Formation Flying Benefits Based on Vortex Lattice Calculations." NASA-CR-151974. 4 April 1977.
- [8] Proud, Andrew W., "Close Formation Flight Control," MS Thesis, AFIT/GE/ENG/99M-24, School of Engineering, Air Force Institute of Technology (AU), Wright-Patterson AFB, OH, March 1999.
- [9] Proud, Andrew W., Meir Pachter and J. J. D'Azzo "Close Formation Flight Control," *Proceedings of the 1999 AIAA Guidance, Navigation and Control Conference*, Portland, OR, August 9-11, 1999, 99-4112.
- [10] Blake, William and Dieter Multhopp, "Design, Performance, and Modeling Considerations for Close Formation Flight," *American Institute of Aeronautics and Astronautics Journal*, 98-4343.
- [11] Myatt, James H. and William B. Blake, "Aerodynamic Database Issues for Modeling Close Formation Flight." *American Institute of Aeronautics and Astronautics Journal*, 99-4194.
- [12] Pachter, M., J.Dargan, J. J. D'Azzo, "Automatic Formation Flight Control," *AIAA Journal of Guidance, Control and Dynamics*, Vol 17, No 6, Nov-Dec 1994, pp 1380-1383.

- [13] Stevens, Brian L., Frank L. Lewis, Aircraft Control and Simulation, John Wiley & Sons, 1992.
- [14] Bertin, John, J. and Michael L. Smith, Aerodynamics for Engineers, Simon & Schuster, 1998.
- [15] Brown, Clinton E., Peter Van Dyke, and John W. Kloetzli, "Measurements and Analysis of the Forces Acting on a Small Aircraft Flying in the Upwash of a Large Transport," USAF Office of Scientific Research Technical Report 7615, April 1978.

## Vita

Captain James K. Hall was born 7 June 1969 in Salt Lake City, UT, where he graduated from Brighton High School in 1987. Captain Hall served a two-year proselytizing mission for the Church of Jesus Christ of Latter-Day Saints in France and Switzerland. He received a Bachelor of Science Degree in Mechanical Engineering from Brigham Young University in Provo, UT on 23 April 1993. After being commissioned a Second Lieutenant in the United States Air Force on 24 April 1993, his first six months of active duty were spent at the maintenance officer course at Sheppard AFB, TX. His first real assignment was as a Maintenance Officer in the 1 FW at Langley AFB, VA. He served as Assistant Officer in Charge (OIC) of the Propulsion Flight, OIC of the Accessory Maintenance Flight, Commander of the Programs Flight, and Contract Field Team (CFT) Project Officer. Captain Hall was next assigned to the F-16 Management Directorate at Hill AFB, UT where he was the systems engineer in charge of sustainment engineering for landing gear and wheels and brakes for the entire F-16 fleet. In December of 1997 he was selected to attend the Air Force Institute of Technology School of Engineering to receive a Masters of Science Degree in Aeronautical Engineering. His follow-on assignment from AFIT is to the Air Force Research Laboratory, Wright-Patterson AFB, OH. Captain Hall is married to the former Angela M. Teames of Salt Lake City, UT. They currently have two children, Jacob--age six and Bailey Jane--age four, with another child due in May of 2000.

Permanent Address:

3113 Bonniebrook Dr.

Plano, TX 75075

REPORT DOCUMENTATION PAGE			Form Approved OMB No. 0704-0188	
Public reporting burden for this collection of information is estimated to average 1 hour per response, including the time for reviewing instructions, searching existing data sources, gathering and maintaining the data needed, and completing and reviewing the collection of information. Send comments regarding this burden estimate or any other aspect of this collection of information, including suggestions for reducing this burden, to Washington Headquarters Services, Directorate for Information Operations and Reports, 1215 Jefferson Davis Highway, Suite 1204, Arlington, VA 22202-4302, and to the Office of Management and Budget, Paperwork Reduction Project (0704-0188), Washington, DC 20503.				
1. AGENCY USE ONLY (Leave blank)		2. REPORT DATE 9 Mar 00		3. REPORT TYPE AND DATES COVERED
4. TITLE AND SUBTITLE THREE DIMENSIONAL FORMATION FLIGHT CONTROL			5. FUNDING NUMBERS	
6. AUTHOR(S) James K. Hall, Capt, USAF				
7. PERFORMING ORGANIZATION NAME(S) AND ADDRESS(ES) AFIT 2950 P Street WPAFB, OH 45433			8. PERFORMING ORGANIZATION REPORT NUMBER  AFIT/GAE/ENY/00M-06	
9. SPONSORING/MONITORING AGENCY NAME(S) AND ADDRESS(ES) William B. Blake AFRL/VACA 2210 8th Street WPAFB, OH 45433			10. SPONSORING/MONITORING AGENCY REPORT NUMBER	
11. SUPPLEMENTARY NOTES Meir Pachter DSN 255-3636 x4593 meir.pachter@afit.af.mil				
12a. DISTRIBUTION AVAILABILITY STATEMENT Approved for public release; distribution unlimited			12b. DISTRIBUTION CODE	
13. ABSTRACT (Maximum 200 words) Automating the control of an aircraft flying in formation necessitates the extension of the theory of formation flight control to allow for three dimensional maneuvers. The formation was modeled as a two-aircraft, leader and wingman, formation. Both aircraft has its own three dimensional, rotating and translating, Cartesian axes system, with special attention being given to the motion of the leader in relation to the wingman. The controller operated using the equations of motion expressed in the rotating reference frame of the wing aircraft. The control system has seven states, three inputs and three disturbance signals to model the dynamics of the formation in three dimensional space. The control law employed was the feedback of the difference between in actual separation distance and the commanded separation distance to affect changes in thrust, lift, and roll rate. The control system incorporated proportional, integral, and derivative control elements, each with separate gains, to achieve and maintain the specified formation geometry despite various maneuvers flown by the leader. Simulated maneuvers included: an initial displacement of the wingman away from the formation geometry, and changes in the leader's velocity, altitude, and heading. For each maneuver, the controller performance was sufficient to maintain the commanded formation geometry.				
14. SUBJECT TERMS Automatic Formation Flight Control; Close Formation Flight			15. NUMBER OF PAGES 93	
			16. PRICE CODE	
17. SECURITY CLASSIFICATION OF REPORT UNCLASSIFIED	18. SECURITY CLASSIFICATION OF THIS PAGE UNCLASSIFIED	19. SECURITY CLASSIFICATION OF ABSTRACT UNCLASSIFIED	20. LIMITATION OF ABSTRACT UL	